CHEMICAL ENGINEERING SCIENCE
GENIE CHIMIQUE

VOL. 2 DECEMBER 1953 NO. 6

De l'importance de la porosité fine du carbone sur sa vitesse de combustion

Communication préliminaire

MAURICE LETORT et ROBERT MAGRONE

Ecole Nationale Supérieure des Industries Chimiques, Université de Nancy, Faculté des Sciences, Nancy, France

(*Received* 1 *October* 1952)

Summary—Fine particles of graphite (90 to 720 μ) were burnt at 500-600°C. At the same time the rate of reaction and the B.E.T. area of the sample were determined. While the experiment is taking place the rate of combustion per cm^2 of B.E.T. surface keeps rising. The evolution of the fine porosity of the particle allows an interpretation of this variation. It is only at the end of the combustion when the particle has become very cavernous that the measured rate of reaction has a definite physical significance. The complications which can happen according to the nature of the porosity and its distribution between the particles are examined. This method and this interpretation are applicable to any gas-solid reaction of the carbon combustion type ; they particularly deal with the problem of coke reactivity.

Résumé—Les auteurs décrivent leur méthode qui consiste à brûler à basse température (500-600°C) jusqu'à disparition complète un échantillon de graphite en très petits grains (90 à 720 μ) calibrés, en déterminant parallèlement la vitesse de réaction et la surface B.E.T. de l'échantillon. Ils donnent pour exemple une courbe de combustion qui correspond à un cas relativement simple. La vitesse de combustion rapportée au cm^2 de surface B.E.T. ne cesse d'augmenter au cours de l'expérience. Ils montrent comment l'évolution de la porosité fine du grain permet d'interpréter cette variation. C'est seulement en fin de combustion, lorsque le grain est devenu très caverneux qu'on peut atteindre et mesurer une vitesse de réaction qui a une signification physiquement définie. Ils examinent rapidement les diverses causes de complications qui peuvent survenir suivant la nature de la porosité et sa distribution entre l'ensemble des grains. La méthode et l'interprétation intéressent toute réaction gaz-solide du même type que celle de la combustion du carbone ; en particulier, elles intéressent le problème de la réactivité des cokes.

Les valeurs données pour la vitesse de combustion du carbone, la composition des produits formés ainsi d'ailleurs que les caractéristiques cinétiques de la réaction varient beaucoup d'un échantillon à l'autre. C'est ainsi que J. R. ARTHUR [1] décrit la combustion de deux lots de carbone (un graphite artificiel et un coke) qui brûlent à la même vitesse alors que l'un est vers 900°C et l'autre vers 600°C ce qui, pour une énergie d'activation d'ARRHENIUS de 40 K. cal. correspondrait, toutes choses égales d'ailleurs, à un rapport de 1 à plus de 10^3 entre les constantes de vitesse attachées, pour la même température, à ces échantillons respectivement.

Nous avons donné [2] de premières raisons de penser qu'indépendamment de la structure cristallographique (graphite ou carbones amorphes) et de la pureté du carbone, la porosité de la masse soumise à la combustion joue un rôle important dans cette dispersion des résultats. La présente étude confirme cette opinion. Elle décrit notre méthode d'étude et propose une interprétation de

l'influence de la porosité fine du combustible sur la vitesse de combustion et sur l'évolution de cette vitesse au cours de l'expérience.

La méthode expérimentale a été décrite antérieurement [3]. Elle se rapproche des conditions habituelles d'utilisation des combustibles solides à la différence qu'elle est à très petite échelle afin que les conditions expérimentales, pression et température, soient strictement définies.

L'appareil est en somme un très petit fourneau construit en verre pyrex ou en silice fondue. Un courant d'air sec et décarbonaté traverse à la pression ordinaire et à un débit de 5 à 15 litres à l'heure une pastille de silice frittée qui porte une couche (de 3 à 6 mm de hauteur et de 2 à 3 cm de diamètre) de grains de graphite Acheson de haute pureté.

Ces grains sont préparés par broyage au mortier d'agate de baguettes, barres ou plaques de graphite,* et séparés par tamisage. Nous avons généralement employé deux calibres de grains le diamètre moyen étant 720 μ (passant au tamis A.S.T. M.20 et refusé au tamis 30) et 90 μ (passant au tamis 140 et retenu sur tamis 200). Les volumes de ces grains sont donc dans le rapport de 500 à 1 environ.

La température de la charge (fixée à $\pm$ 0·5° près) est choisie pour que la combustion soit très lente (plusieurs dizaines d'heures pour brûler 0·5 gr.). Cette condition est indispensable, comme on l'a reconnu depuis longtemps, pour être assuré que la vitesse mesurée n'est pas celle de phénomènes occasionnels de diffusion du réactif gazeux dans le lit de combustible. Nous allons montrer toutefois, ce qui semble-t-il est original, que cette condition n'exclut pas le rôle, qui est déterminant, de la diffusion à l'intérieur du grain.

Pour ces basses températures, le gaz qui sort du four contient un large volume d'oxygène qui n'a pas réagi, environ 1% en volume de CO^2 et 0·1 à 0·4% en volume de CO. C'est dire qu'il se fait à la fois CO^2 et CO. Le rapport des concentrations de ces oxydes varie beaucoup d'un graphite à l'autre ; par exemple, le rapport $\frac{[CO]}{[CO] + [CO_2]}$ est 0·4 pour un graphite artificiel que nous avons longuement etudié alors qu'il est inférieur à 0·1 pour un graphite naturel (Madagascar) dans les mêmes conditions. Nous n'avons pas encore examiné la question de savoir si cette composition correspond aux produits primaires de la réaction, ce qui paraît d'ailleurs peu probable.

La teneur en CO et CO^2 du gaz de réaction (que nous déterminions antérieurement par microgravimétrie [3] est mesurée maintenant de façon continue par absorption du rayonnement i.r. Il est facile d'en déduire la masse de carbone gazéifiée en un temps donné (une min par exemple); cette masse définit la *vitesse de combustion* V.

La figure 1 donne cette vitesse en fonction de la durée de l'expérience ; elle représente à titre d'exemple la combustion à 609°C de 0·5 gr. d'un échantillon (immatriculé AFC.1) de graphite Acheson pur (0·02% de cendres) sous les deux calibres de grains. Ces grains n'avaient subi aucun traitement (de dégazage par exemple) avant d'être soumis à la combustion. Il est important de remarquer sur les courbes de cette figure que l'expérience a été poursuivie jusqu'à disparition complète du combustible ($V = 0$) ; nous verrons bientôt l'intérêt de cette façon de procéder.

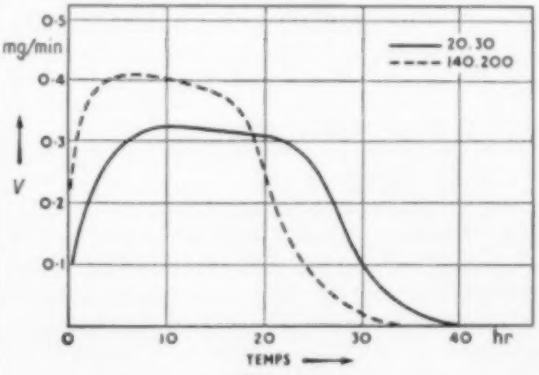

Fig. 1.

D'autres échantillons, également de haute pureté et d'origine analogue, ont été essayés dans les mêmes conditions. Les courbes obtenues bien qu'elles présentent des analogies sont nettement

* Nous adressons nos remerciements à la Compagnie PECHINEY qui a bien voulu nous fournir gracieusement ces échantillons.

VOL. 2 1953

différentes entre elles, en particulier du point de vue quantitatif. En fait, *chaque lot examiné fournit une courbe qui lui est particulière.*

D'autre part, pour un lot déterminé, on est bien embarrassé pour définer une vitesse de combustion caractéristique puisque cette vitesse ne cesse de varier dans d'importantes proportions d'un bout à l'autre de l'expérience comme le montre la figure 1. Ainsi, les combustions complètes auxquelles nous nous sommes astreints montrent l'inanité des vitesses " stationnaires " (en fonction du temps) qu'on pourrait espérer atteindre par expérience directe.

De fait, pour une réaction hétérogène, l'expression d'une vitesse de réaction n'a de sens que si elle est rapportée à l'aire qui participe à la réaction. Afin de connaître celle-ci, la surface réelle de la charge de graphite a été mesurée grâce à la méthode classique de BRUNAUER, EMMETT et TELLER (B.E.T.) par adsorption de méthane (ou d'azote) à — 195°C.*

La mesure effectuée sur la charge de graphite avant combustion montre que l'aire réelle des grains est beaucoup plus grande que leur surface géométrique ; pour le lot AFC 1 auquel se rapporte la fig. 1, le " facteur de rugosité " est 70 sur le grain fin et 220 environ sur le gros grain.

Le grain est donc poreux. Cette observation essentielle est recoupée par d'autres faits : branches d'hystérèse que manifestent les isothermes d'adsorption dans la mesure des surfaces B.E.T., lenteur de pénétration du benzène dans le grain lors de la détermination picnométrique de densité du graphite, diffusion aux petits angles des rayons X par le graphite.

Après qu'elle a subi une combustion d'une durée déterminée, la charge de graphite est sortie du four, pesée et on en mesure à nouveau sa surface B.E.T. De la sorte, la construction d'une courbe complète de combustion exige une longue expérimentation, mais il paraît indispensable de consentir cet effort si l'on veut comprendre le mécanisme de la combustion et mesurer une vitesse qui soit physiquement définie.

Le document le plus important que fournit cette étude est représenté sur la figure 2 où la vitesse de combustion V (en mg de carbone gazéifié par min) du lot AFC 1 est portée en ordonnée et la surface B.E.T. (m^2) en abcisse S. Pour être complet ce graphique pourrait comporter suivant une troisième coordonnée l'indication de la masse brûlée à chaque instant : celle-ci est représentée par les diverses valeurs m portées sur le plan et qui varient de $m = 0{\cdot}5$ gr (instant initial) à $m = 0$.

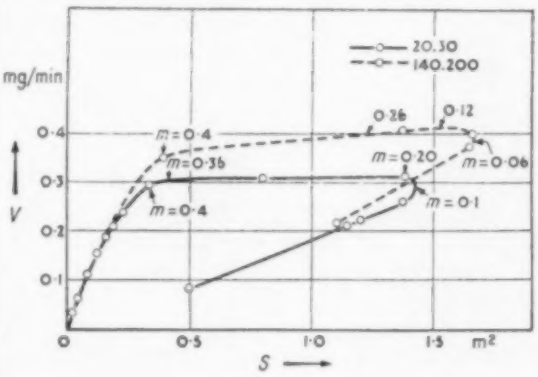

Fig. 2.

On distingue aisément sur ces courbes trois parties que nous commenterons pour exemple sur la courbe en trait plein qui représente la combustion du grain 20-30. Cette courbe montre :

1°/ Une phase initiale qui s'étend jusqu'à ce que 20% de la charge soit brûlée ($m = 0{\cdot}1$ gr) ; la surface B.E.T. ainsi que la vitesse de réaction augmentent et, approximativement, dans le même rapport.

2°/ Une phase intermédiaire qui va jusqu'environ 80% de la masse brûlée ($m = 0{\cdot}4$ gr) ; S diminue considérablement tandis que V varie très peu. Il faut spécialement remarquer au début de cette phase une partie de la courbe qui apparaît peu sur cette figure bien qu'elle corresponde à 20% de la diminution de masse (de $m = 0{\cdot}1$ gr à

* Ces mesures ont été effectuées par Mr. LUCIEN BONNETAIN que nous remercions bien vivement. Signalons à ce propos que le type nouveau et très particulier d'isothermes d'adsorption qui a été découvert à cette occasion (L. BONNETAIN, X. DUVAL et M. LETORT C.R. 1952 **234**, 1363) vient d'être confirmé indépendamment (M. H. POLLEY, W. D. SCHAEFFER et W. R. SMITH, J. Phys. Chem., 1953 **57** 469).

$m = 0{\cdot}2$ gr) et pour laquelle S commence à diminuer alors que V continue à croître.

3°/ Une phase finale qui se termine nécessairement à l'origine des coordonnées ; S et V diminuent concomitamment, la porportionnalité de ces deux grandeurs étant exactement vérifiée dans la partie extrême de la courbe, c'est-à-dire en fin d'expérience.

Il est facile de reprendre les points expérimentaux de cette figure sous une autre forme. Dans ce nouveau graphique, (fig. 3) nous donnons, en fonction de la masse consumée, la vitesse de réaction $V°$ *rapportée au* m² *de surface B.E.T.*

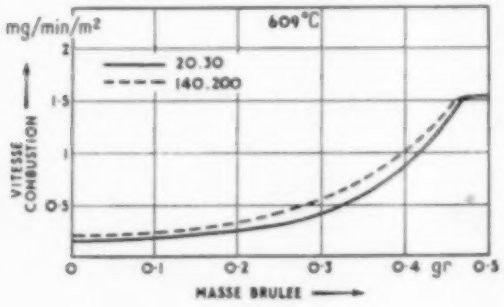

Fig. 3.

Nous retrouvons évidemment les trois phases que nous venons de dire. Jusqu'environ 20% de masse brûlée, cette vitesse $V°$ est à peu près constante et de l'ordre de 0·2 mg/min. m² ; puis elle augmente assez vite pour se fixer à la valeur constante de 1·5 mg/min m² qui n'est d'ailleurs atteinte que lorsque plus de 95% de la charge sont disparus. Il est intéressant d'observer que cette valeur limite est la même pour les deux calibres de grains.

L'essentiel de l'interprétation tient dans l'idée très simple que *toute l'aire mesurée par la méthode B.E.T. ne participe pas nécessairement à la combustion.*

Sans doute, toute cette surface est-elle accessible aux gaz puisque la mesure par adsorption qu'on en fait est précisément fondée sur l'accès d'un gaz à la surface, et il n'y a aucune raison de penser que la surface décelée par adsorption ne soit pas également accessible aux gaz à la température de combustion. Encore faut-il pour que la combustion ait lieu en un endroit donné de la surface que l'oxygène puisse parvenir jusqu'à cet endroit. Or, l'oxygène peut être complètement consommé avant de l'atteindre.

D'une façon plus générale, suivant l'endroit considéré de la surface, les conditions expérimentales à un instant donné de la combustion peuvent être très différentes. A ce propos, nous avons à examiner trois facteurs : nature (et état) de la surface à l'endroit considéré, température et pression de l'oxygène en ce lieu.

On ne voit pas de raison pour que l'activité propre de la surface ne soit pas la même en chaque point ; nous admettrons donc que la fraction active (qui peut être très petite) de l'unité d'aire est partout identique à un instant donné (ce qui ne veut pas dire, que celle-ci reste nécessairement égale à elle-même pendant toute la durée de l'expérience).

Nous négligerons de même l'éventuelle différence de température qui pourrait exister entre le cœur et la périphérie du grain du fait de l'exothermicité de la réaction, le centre pouvant être plus chaud que la surface. Nous avons toutes raisons de croire en effet qu'à ces très faibles vitesses de combustion, l'équilibre thermique est réalisé entre tous les grains de la charge et dans chaque grain considéré isolément.

Par contre, si l'on veut bien considérer que l'oxygène qui diffuse depuis l'entrée d'un pore vers le fond (tandis que les produits de la réaction diffusent en sens inverse) est nécessairement consommé pendant ce cheminement, on doit admettre que, suivant la profondeur du point considéré sur la paroi du pore, la pression de l'oxygène peut prendre toutes les valeurs depuis la pression de ce gaz dans l'air à la pression ordinaire (1/5 atm) jusque zéro.

La vitesse globale qu'on mesure étant la somme de toutes les vitesses locales, il conviendrait de connaître en chaque point de la surface la valeur de la vitesse de combustion en fonction de la pression d'oxygène en ce point. A ce titre, nous nous représentons la combustion du grain de la façon suivante.

Jusqu'à une certaine profondeur dans le pore, la pression d'oxygène reste suffisante pour que

l'acte d'adsorption de ce gaz soit extrêmement rapide comparativement à la vitesse de transformation chimique en phase adsorbée ou à la vitesse de désorption. Jusqu'à cette valeur de la pression c'est à dire jusqu'à cette profondeur dans le pore, la vitesse de réaction serait donc indépendante de la pression d'oxygène (ordre zéro) et identique en tout point de la paroi. Il existerait ainsi autour du grain une sorte *d'écorce*, plus ou moins épaisse suivant la température, à l'intérieur de laquelle toute la surface serait soumise à une vitesse *bien définie* de combustion. Cette écorce est vraisemblablement d'autant plus mince que la température est plus élevée puisque la consommation de l'oxygène qui diffuse dans un pore est évidemment d'autant plus rapide que la température est plus grande.

Au delà de cette écorce en allant vers l'intérieur du grain, la pression d'oxygène se trouvant très sensiblement diminuée, l'ordre zéro ne serait plus respecté mais tendrait progressivement, à mesure que la pression p_{O_2} locale s'abaisse, vers l'ordre 1 qui serait effectivement atteint pour les plus basses pressions d'oxygène. Ainsi, sous l'écorce à l'intérieur de laquelle chaque cm² de surface brûle à la même vitesse, il existerait une zone où la vitesse locale de combustion diminuerait progressivement jusqu'à devenir nulle.*

Ainsi la vitesse globale mesurée (qui représente, nous le rappelons, une masse de carbone gazéifié par min) serait la somme de deux termes que nous désignerons pour simplifier par vitesse de combustion " en régime externe " et vitesse de combustion " en régime interne," ce second terme étant l'intégrale définie d'une infinité de vitesses locales variables suivant le point considéré. La vitesse locale moyenne de la zone interne étant nécessairement plus petite que la vitesse locale (identique en chaque point) de la zone externe, pour que ce second terme ne soit pas négligeable vis à vis du premier, il faut penser que la zone de combustion, " en régime interne " est épaisse par rapport à l'écorce qui brûle " en régime externe."

Cette représentation permet de rendre compte très simplement des résultats expérimentaux.

Ainsi, pour la courbe que nous avons commentée (fig. 2 : grain 20-30), dans la phase initiale de la combustion, il s'exerce une intense corrosion du grain qui multiple par 3 environ la surface de celui-ci (pour 0·5 gr de graphite, S passe de 0·5 à 1·4 m²). La réaction se fait essentiellement en régime de " combustion externe." La proportionnalité entre V et S est approximativement respectée, surtout en début de combustion.

Mais le développement de la surface ne se poursuit pas indéfiniment. L'enlèvement de matière intervient en sens inverse de l'effet de corrosion : le détail du phénomène est évidemment fort complexe mais, au total, on constate qu'entre 20 et 80% de la consommation complète de la charge, la surface diminue de 1·4 à 0·35 m². Cependant la vitesse de combustion ne varie que très peu pour la raison que la corrosion a augmenté et ne cesse d'augmenter l'accessibilité des pores à l'oxygène. De façon générale, les parties très enfoncées de la surface qui ne brûlaient pas, tendent à mesure qu'elles se découvrent, à se consumer d'abord en régime de combustion " interne," puis, le pore s'étant creusé davantage, en régime de combustion " externe " c'est à dire au maximum de vitesse. C'est là le fait essentiel.

Enfin, le grain étant devenu très caverneux, toute la surface brûle au maximum de vitesse. La pression locale p_{O_2} est la même en chaque point. Il y aurait-il des différences de pression d'un endroit à un autre que celles-ci ne se traduiraient plus sur la vitesse locale qui obéit partout à l'ordre zéro. On est ici dans la phase finale de la combustion. Elle correspond à un cas très simple. En effet, tout se passe comme si on substituait au grain caverneux un grain absolument compact et de même surface (réelle). La proportionnalité entre V et S est exactement vérifiée pour les derniers temps de l'expérience.

Au total, la corrosion du grain permet donc d'interpréter de façon rationnelle l'évolution de la vitesse de combustion en fonction du temps. Dans l'état actuel de nos recherches, rien n'autorise cependant à croire que la corrosion du grain

* Le calcul permet de préciser qu'à mesure qu'on se déplace depuis l'entrée du pore vers le fond, p_{O_2} décroît d'abord suivant une parabole dans toute la zone où l'ordre zéro est vérifié ; puis cette courbe tend vers la forme d'une exponentielle qui serait effectivement atteinte lorsque la réaction devient d'ordre 1.

soit la raison *exclusive* de cette évolution. On peut concevoir que, parallèlement, l'état de surface de l'unité d'aire se modifie spontanément, par exemple par formation d'une couche adsorbée inhibitrice. Des recherches dans ce sens ne pouvaient toutefois être entreprises utilement avant que l'influence de la porosité n'ait été elle même clairement reconnue.

Il est important de remarquer enfin que c'est seulement dans la dernière partie de la phase finale de la combustion que la vitesse observée prend une signification physiquement définie car, à ce moment, la surface B.E.T. participe *totalement et de la même façon* à la combustion. Pour les autres parties de la courbe de combustion, la distribution des vitesses locales de réaction et la part de la surface B.E.T. qui intervient réellement dans la combustion, sont inconnues.

On arrive ainsi à la conclusion d'apparence paradoxale (du moins pour le graphite que nous étudions ici ou des graphites analogues) que c'est seulement lorsque la quasi-totalité de la charge est brûlée qu'il est possible d'atteindre et de mesurer la vitesse de l'acte chimique dans des conditions définies, grandeur que nous proposons d'appeler " vitesse *réelle* de combustion " V_r. Cette conclusion justifie à posteriori notre méthode qui consiste à brûler *toute* la charge.

Pour le graphite AFC.1 que nous venons d'examiner, cette vitesse absolue est égale à $1{\cdot}25\ 10^{14}$ atomes/cm² sec à 609°C.

Toutefois, il semble qu'il subsiste des différences sensibles entre les vitesses réelles de combustion V_r de divers graphites. L'examen systématique de nombreux lots de provenances diverses permettra de préciser ce point. Ces différences ne doivent pas surprendre ; il est concevable en effet que la fraction active de l'unité de surface dépende de la structure cristallographique du carbone (degré de graphitation). L'état de surface en fin d'expérience peut d'autre part varier d'un graphite à l'autre.

Quoi qu'il en soit, ces écarts (qui, dans l'état actuel de nos recherches, paraissent être de l'ordre d'un facteur de 2 ou 3) sont petits comparés aux différences beaucoup plus considérables que l'on constate entre des vitesses *brutes* de combustion et que nous attribuons essentiellement aux effets de la porosité.

L'exemple du graphite AFC. A a été choisi car il correspond à un cas relativement simple et fondamental. D'autres échantillons fournissent des résultats plus compliqués et dont l'interprétation est moins simple. Toutefois, l'analyse qui précède du mécanisme de combustion du grain reste non seulement valable mais elle constitue l'indispensable clef des nouveaux problèmes qui se posent.

En effet, comme on peut logiquement l'attendre au terme de cette analyse, les différences de porosité doivent nécessairement se traduire dans les courbes de combustion. Ces différences – et les complications qu'elles entraînent – paraissent provenir essentiellement de trois causes :

1°/ Le diamètre initial moyen des pores est plus ou moins large, l'influence de la diffusion dans les pores étant d'autant plus marquée que la porosité est plus fine.

2°/ Les pores ont grossièrement le même diamètre ou, au contraire, les dimensions de ces diamètres sont largement dispersées.

3°/ Les pores sont distribués de façon sensiblement uniforme dans la masse du graphite ou, au contraire, certains grains sont notablement plus poreux que d'autres, de sorte que la charge se comporte comme un mélange de diverses qualités de grains. Cette hétérogénéité de distribution entre les grains intéresse le nombre des pores et (ou) leurs dimensions.*

Le problème peut donc se présenter sous des aspects extrêmement complexes. Nous n'examinerons pas ici ces complications. C'est essentiellement la méthode de travail que nous désirions exposer. Nous indiquerons seulement que le graphite (AFC.1) dont nous avons commenté la combustion possède des pores très fins, à peu près analogues entre eux et distribués de façon uniforme dans la masse ; ces deux dernières caractéristiques justifient que nous le considérions comme un cas relativement simple.

* De fait, des diverses causes de complications ne sont pas indépendantes ; ainsi, il semble que la présence de pores très larges s'accompagne toujours d'une distribution non uniforme de la porosité entre l'ensemble des grains.

VOL. 2 1953

Il va sans dire enfin que cette méthode de travail et cette interprétation ne se limitent pas au cas graphite que nous n'avons choisi que pour disposer d'un combustible bien défini et éliminer ainsi (ou du moins considérablement diminuer) l'influence d'autres facteurs tels que la structure cristallographique et la pureté chimique. Elles intéressent toutes les réactions hétérogènes du même type (reaction gaz – solide avec formation de produits gazeux). En particulier, dans le domaine de la combustion du carbone, elles intéressent directement une étude rationnelle du problème depuis longtemps posé de la réactivité des cokes.

L'un de nous (R.M.) adresse ses très sincères remerciements à la *Cie Pechiney* pour l'assistance financière qu'il a reçu de celle-ci pendant toute l'exécution de ce travail.

BIBLIOGRAPHIE

[1] ARTHUR, J. R.; Trans Faraday Soc. 1951 **47** 164.
[2] LETORT, M. et MAGRONE, R.; J. Chim. Phys. 1950 **74** 576.
[3] LETORT, M. et coll.; J. Chim. Phys. 1950 **47** 548.

Chemical Engineering Science, 1953, Vol. 2, pp. 240 to 246. Pergamon Press Ltd.

Mixing of solid particles

R. Blumberg and J. S. Maritz*

National Chemical Research Laboratory, South African Council for Scientific and Industrial Research, Pretoria

(*Received* 1 *September* 1953)

Summary—The theoretical concepts of complete and incomplete mixing have been discussed, and a definition for complete mixing has been proposed, using a statistical hypothesis as the test criterion. The application of this has been confirmed experimentally and it has been shown that, with random sampling, n, the number of particles in a sample, and x, the proportion of particles of type A in the sample, follow normal distributions.

It has further been shown that a small number of samples examined statistically, is sufficient to indicate whether or not mixing is complete at any time during the mixing process, and that the progress of mixing with time may be followed statistically.

Résumé—Après avoir discuté les concepts théoriques de " mélange imparfait " et de " mélange parfait," l'auteur propose une définition du " mélange parfait " posant à la base du critère expérimental une hypothèse statistique. L'expérience est en accord avec cette hypothèse : elle montre que le nombre de particules n, est la proportion x des particules du type A dans l'échantillon, obéissent à une loi de distributions normales, lorsque les échantillons sont choisis au hasard.

De plus, l'auteur établit que, durant l'opération du mélange, l'examen statistique d'un petit nombre d'échantillons indique si le mélange est ou n'est pas parfait à un instant donné : il est donc possible, par l'observation statistique, de suivre les progrès du mélange en fonction du temps.

1. Introduction

Although during the past 20 years a large number of papers have been published dealing with various aspects of mixing, the fundamentals of solid-solid mixing have barely been touched. In view of the application of the dry mixing operation to many widely different processes, it was felt that additional fundamental work was warranted.

A study of the literature showed that there have been two lines of approach to the problem of solid-solid mixing thus far. Brothman and co-workers [1] and Coulson and Maitra [2], [3] approached the problem from the kinetics viewpoint, while Lacey [4], Buslik [5] and De Jong [6], all adopted the statistical approach using the value of the standard deviation as the mixing criterion. Of all these workers, only Coulson and Maitra, and Lacey, published experimental results in support of their hypotheses.

Lacey was concerned with degree of mixing, and in his experimental work used small batches of relatively large (0·2 in. diameter) coloured spheres. After mixing, he examined the *whole* batch by dividing it into small samples, without disturbing the relative positions of the particles, and counted the particles in each sample. Since the entire batch was examined, the question of sampling did not come up for consideration. Lacey concluded that it was probably impossible to express the state of a mixture adequately by a single number, but that it could be expressed by a line on a suitable graph, and that this would provide a quantitative as well as a qualitative method of comparing mixtures and the performances of mixing machines.

Coulson and Maitra examined the main factors influencing the rate of mixing and concluded that their basic kinetic mixing equation applied over a wide range of conditions, but had certain definite limitations.

The kinetic approach offers considerable possibilities of practical application, but Coulson and

* Present address : Transvaal Chamber of Mines Research Laboratories, Kew Road, Richmond, Johannesburg.

Maitra omitted to refer to the statisical standards on which their conclusions were based; they simply state that, if n samples out of 30 were found to have approximately the same composition as the whole system, then the mixture was $\frac{n}{30} \times 100\%$ mixed. Lacey's method cannot be applied in practice, because of the impossibility of sampling and counting an entire batch.

It was felt that the first stage in a fundamental examination of the unit operation of solid-solid mixing should be to define complete mixing, to settle the question of adequate sampling, and to arrive at a means of expressing to what extent a mixture approached the completely mixed state.

2. Equipment

The purpose of these experiments being an investigation of mixing fundamentals, and not of mixer characteristics, it was considered advisable to use a very simple type of mixer. The design of Coulson and Maitra was followed in this connection, a simple Perspex drum 6 in. diameter x 9 in. being used. The assembled equipment is shown in Fig. 1.

For the same reason it was thought desirable that differences in physical properties of the materials being mixed should not enter into the investigation at this stage. A closely sized batch of washed Cape sand of uniform quality was therefore divided into two portions, the one dyed blue and the other red; these coloured sands were used for the experiments. They differed in colour only, and this property could have no effect on the mixing of the particles. A summary of physical properties of the sand is given in Table 1.

Table 1. *Physical properties of Cape sand.*

Particle size range : Tyler mesh	−35 +48	−48 +65
Bulk density : g/cc	1·60	1·46
Specific gravity : 20°C	2·631	2·634
% Voids	39	44

The sampling device is shown in Fig. 2. It consisted of a rod 0·132 in. diameter with 9 cavities of 0·0635 in. diameter drilled at 1 in. intervals along its length to a depth of 0·0635 in. The first cavity was 0·43 in. from the end. The rod was a sliding fit inside an outer sleeve, which had a strip 0·076 in. wide cut away along its

Fig. 2. Sampler.

length so that the cavities in the rod could be either covered or open. The sampler guide, shown in Fig. 3, could be fitted across the top

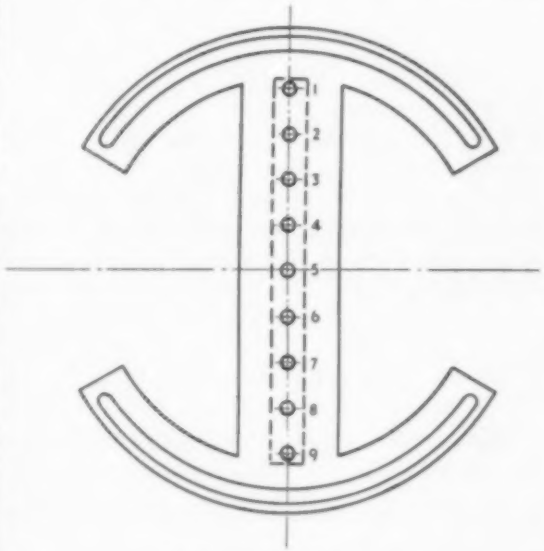

Fig. 3. Sampling guide.

of the drum along any diameter, and the sampler inserted. The fact that the material being mixed consisted of discrete particles created distinct sampling problems and necessitated a standardised sampling procedure throughout, so as to cause as little disturbance as possible in the mixture.

3. Complete Mixing

Fundamental ideas concerning the completely mixed state

Before it was possible to examine the progress of mixing or the degree of mixing achieved, it was considered necessary to define the completely mixed state.

For the experimental work, the sampling instrument was so designed that it withdrew at each position a very small proportion of the total batch, and the sampling could therefore be regarded as having taken place at a "point" in the batch. The first assumption which was made was that if, after a certain set of operations, a sample were withdrawn consisting of n particles of which r were red, and if the same procedure were repeated a number of times, in each case starting from the same datum level, then for a fixed value of n, corresponding to each sampling point, r would be a statistical variable with distribution

$$p(r) = \binom{n}{r} \theta^r (1-\theta)^{n-r} \qquad (1)$$

θ being a parameter called " the probability of drawing red at a certain point."

In the experimental practice it was impossible to draw exactly n particles at each point, so that n also was a statistical variable. The joint distribution of r and n could therefore be expressed by

$$p(r, n) = \binom{n}{r} \theta^r (1-\theta)^{n-r} p(n) \qquad (2)$$

Making use of the normal approximation to the binomial distribution [7], and writing

$x = \frac{r}{n}$ = the proportion of red particles in the sample,

the joint distribution of x and n became

$$p(x, n)\,\mathrm{d}x\mathrm{d}n = \frac{n^{\frac{1}{2}}}{\sqrt{2\pi\theta(1-\theta)}} \exp\left\{-\frac{1}{2}\frac{n(x-\theta)^2}{\theta(1-\theta)}\right\} p(n)\,\mathrm{d}x\mathrm{d}n \qquad (3)$$

In the derivation of this distribution it was assumed that the distributions of both r and n could be approximately represented by continuous ones.

From equation (3) the following results were obtained :

$$E(x) = \mu_1'(x) = \theta \text{ (as was to be expected)}$$
$$\mu_2(x) = \theta(1-\theta)\,E(n^{-1})$$
$$\mu_3(x) = 0$$
$$\mu_4(x) = 3\theta^2(1-\theta)^2\,E(n^{-2})$$

consequently

$$\beta_1(x) = 0$$
$$\beta_2(x) = \frac{3\theta^2(1-\theta)^2\,E(n^{-2})}{\theta^2(1-\theta)^2\,[E(n^{-1})]^2} = \frac{3E(n^{-2})}{[E(n^{-1})]^2}$$

By making the reasonable assumption that $\frac{\mathrm{var}(n)}{[E(n)]^2}$ would be small, it could be shown that

$$E(n^{-1}) \doteq \frac{1}{E(n)}$$

$$E(n^{-2}) \doteq \frac{1}{[E(n)]^2}$$

from which

$$\beta_2(x) \doteq 3$$

i.e., the distribution of x would be approximately normal with

$$\text{mean} = \theta$$

$$\text{variance} = \frac{\theta(1-\theta)}{E(n)}$$

It seemed reasonable to define the completely mixed state as that which would obtain when the probability of drawing red at a certain point was the same at all points in the mixer, i.e., for a completely mixed batch, the values $x_1 \ldots x_k$ obtained by random sampling from the batch, could be regarded as k independent statistical variables each with the same normal distribution.

The first set of experiments was designed to obtain some empirical verification of the above theories.

Experimental Procedure

The drum was held in the vertical position and red sand, 500 g, poured in evenly on the bottom. Blue sand, 500 g, was then poured in a layer of uniform thickness on top, and the drum attached to the stationary turntable. The angle of tilt of the drum and the speed of rotation were arbitrarily selected, taking into account the findings of Coulson and Maitra. In all this work the drum was rotated at 55 r.p.m. at an angle of 30° from the horizontal until it was judged that the mixing was complete. The mixer was then stopped, and random samples were extracted using the sampler. The individual samples were

VOL. 2 1953

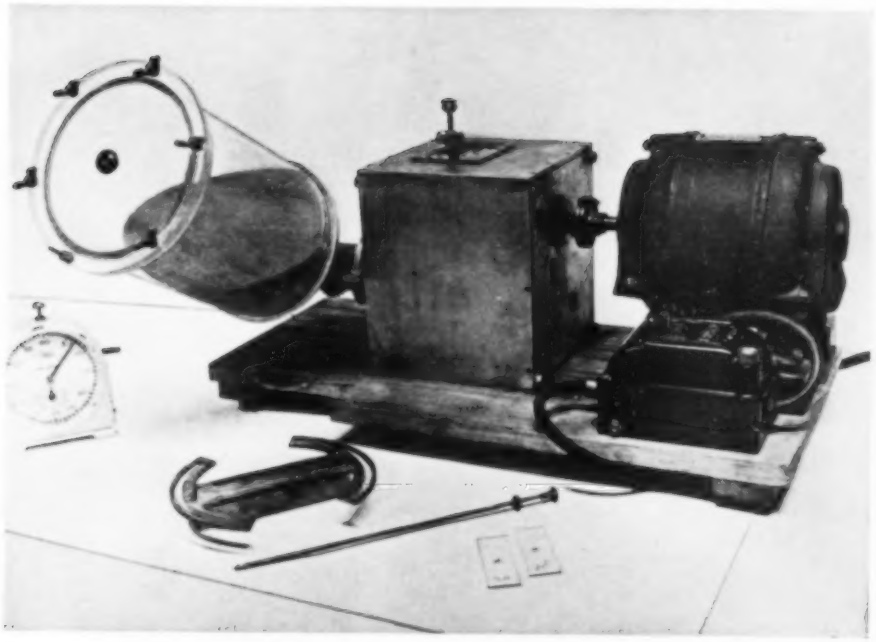

Fig. 1. Mixer and auxiliary equipment

transferred to separate cavity slides, the particles projected on to the screen of a Vickers projection microscope, using oblique incident light and magnification 12 ×, and the number of red and blue particles in each sample counted. The small quantity of sampled sand was returned to the drum, rotation started and continued for a similar period of time. Then the mixture was again sampled. In this type of test at least 160 samples were examined and the particles counted.

Discussion of Results

When a distribution of n was examined, it was found in fact to be almost normal with a mean ($\bar{n}$) of 72·3 and $\frac{S_n^2}{n^2}$ small (= 0·005). The next step was an examination of observed distributions of x. One such distribution is given in Table 2, together with the appropriate calculated normal frequencies. It will be noted that agreement between observed and calculated frequencies is good, and acceptable according to the x^2 test. This lends confidence to the formulae derived for the mean and variance of the expected distribution, as well as for its shape.

Table 2. Distribution of x observed frequencies after complete mixing, together with calculated normal frequencies as found from

$$p(x) = \frac{1}{\sigma\sqrt{2\pi}} \exp.\left[-\frac{1}{2}\left(\frac{x-\xi}{\sigma}\right)^2\right] \quad \text{with } \xi = 0{\cdot}5 \text{ and } \sigma = 0{\cdot}5/\sqrt{72{\cdot}3}.$$

x	Observed frequency		Calculated frequency	
·655–·690	2		·7	
·620–·655	3	18	2·7	12·1
·585–·620	13		8·7	
·550–·585	19		19·8	
·515–·550	31		32·2	
·480–·515	32		37·9	
·445–·480	32		31·1	
·410–·445	16		17·8	
·375–·410	9		7·5	
·340–·375	3	13	2·1	10·1
·305–·240	1		·5	

$$x^2 = 4{\cdot}91$$

$$\text{d. f.} = 6$$

$$P\{x_6^2 > 4{\cdot}91\} = {\cdot}57$$

4. Incomplete Mixing

Theoretical considerations

On the basis of the definition for complete mixing, it follows that mixing would be incomplete if the probability (θ) of drawing red were not identical at all points in the mixer. Therefore, if mixing were incomplete and samples were withdrawn at points $P_1 \ldots\ldots P_k$, then $x_i\,(i = 1 \ldots . k)$ would be normally and independently distributed with means θ_i and variances $\frac{\theta_i(1-\theta_i)}{\nu}$, where $\nu = E(n)$. The calculations are simplified if the variables x_i are transformed [8], [9] to new variables z_i according to

$$z_i = 2 \text{ arc sin } \sqrt{x_i}$$

For ν fairly large, the effect of this is that at points $P_1 \ldots\ldots P_k$ variables z_i would be observed which would be approximately normal with means ζ_i and variances $\frac{1}{\nu}$.

Some measure of the variation between the ζ_i would be a measure of the degree of mixing, based upon the information obtained from points $P_1 \ldots . P_k$. If mixing were complete $\zeta_1 = \zeta_2 = \zeta_3 \ldots\ldots \zeta_k = \zeta_0$ (where ζ_0 is the transform of the total proportion of red in the batch) and it follows that $\phi = \nu \sum_{i=1}^{k} (z_i - \zeta_0)^2$ would be a x^2 variable. This could be used as a test criterion for the statistical hypothesis H_0 : $\zeta_1 = \zeta_2 = \ldots\ldots \zeta_k = \zeta_0$, i.e., as a test for completeness of mixing.

If it were necessary to reject the H_0 hypothesis and therefore to conclude that mixing were not complete, the matter would have to be considered further. Although a "mixing index" is useful in practice, it is quite arbitrary, and, as has been mentioned above, Lacey concluded that it was probably impossible to express the state of a mixture adequately by a single number.

When mixing is incomplete, what appears to be important fundamentally is not the degree of mixing but rather the approach of the mixture towards the completely mixed state. As a means of determining this, ϕ may be used.

A set of experiments was carried out to obtain data to test the theories outlined above.

Experimental Procedure

The drum was filled as described previously, then attached to the stationary turntable at 30° to the horizontal. Definite sampling points were selected as shown in Fig. 4, the positions being

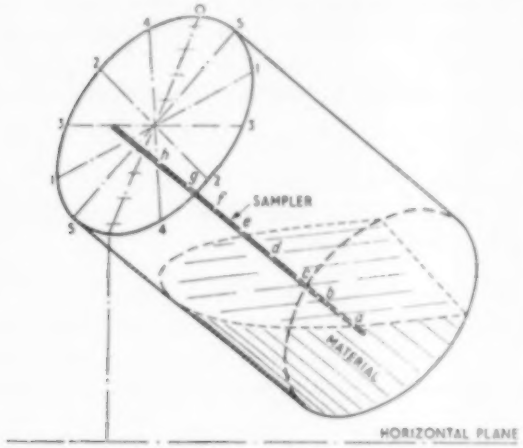

Fig. 4.

located in relation to the horizontal fixed base of the mixer assembly. The batch was sampled before rotation was started, and the samples analysed by counting. The drum was then rotated for 20 seconds at 55 r.p.m., stopped and sampled. This mixing and sampling procedure was repeated a number of times as shown in Table 3. At each sampling approximately 90 separate samples were examined. The sand removed as samples in this test was not returned to the drum, as over the whole experiment it formed only 0·3% of the total batch.

Table 3. Experimental mixing times.

Sampling series No.	*Period of drum rotation – secs.*	
	Actual	*Cumulative*
I	0	0
II	20	20
III	20	40
IV	20	60
V	30	90
VI	30	120
VII	30	150
VIII	30	180
IX	60	240
X	60	300

Discussion of Results

Adequacy of sampling

In the section on the theory of incomplete mixing, it was assumed that k samples would be withdrawn at points $P_1 \ldots\ldots P_k$. Increasing the number of these sampling points would increase the amount of information about the state of the mixing, but for practical reasons this number must be kept small. The question, therefore, was whether a small number of points could give a true picture of the state of the mixing.

It was considered reasonable to assume that after a period of mixing, the variation of θ in the mixer would be continuous. Further, there appeared to be no *a priori* reason for supposing that at any stage during the mixing process this continuous variation of θ would be a systematic fluctuation which would have the value θ_0 at all the arbitrarily selected sampling points. Such a thing, while patently possible, could be regarded as extremely unlikely. Assuming that with the sampler used, the batch contained a total of N possible sampling points (N would be a very large number) and that at a proportion Q of these points $\theta = \theta_0$ (where θ_0 is the total proportion of red particles in the mixer), while at the others $\theta \neq \theta_0$, then if S sampling points were selected, the chance of selecting all these at points at which $\theta = \theta_0$ is $(Q)^s$. Now if $S \geqslant 10$, then even for Q as large as 0·5 this chance is $\leqslant 0{\cdot}001$.

In the experiment under consideration the estimate of ν was 72·3 (*cf.* 3, Discussion of Results). After 60 seconds of mixing, samples were withdrawn from 89 points and calculations gave $\phi = 261{\cdot}0$. According to tables of the x^2 distribution $P\{x^2_{89} \geqslant 261\} < {\cdot}001$, so that, choosing a critical level of 0·01, H_0 had to be rejected. The calculation was repeated using only 10 of the sampling points. These were selected so that at zero time $\theta = 0$ for 5 of the points and $\theta = 1$ for the other five. As shown in Table 4, the result for these 10 points was $\phi = 66{\cdot}7$ and $P\{x^2_{10} \geqslant 66{\cdot}7\} < {\cdot}001$, so that again H_0 had to be rejected.

Similar calculations after 150 seconds of mixing resulted in :

84 points: $\phi = 79{\cdot}7$, $P\{x^2_{84} \geqslant 79{\cdot}7\} > {\cdot}60$; H_0 accepted.

VOL. 2 1953

10 points: $\phi = 14{\cdot}1$, $P\{x^2_{10} \geqslant 14{\cdot}1\} > {\cdot}10$; H_0 accepted.

In both cases the 10 points gave the same result as the much larger number of points. Although this is not a rigorous proof, it does give some confidence for using the smaller number of points and for regarding as reliable any conclusions, concerning the degree of mixing of the batch, which may be based upon them.

Process of Mixing

Having decided that it was possible, on the basis of 10 sampling points to conclude whether or not mixing was complete at the time of sampling, values for ϕ were calculated for various times during the experiment. Results are given in Table 5, and have been plotted against time in Fig. 5. Information about the progress of mixing with time may be obtained from this plot by noting the rate at which the graph approaches k. Thus it appears that after 120 seconds, mixing was practically complete, as at that time ϕ approached its theoretical asymtotic value of 10.*

Table 4. Typical calculation of ϕ (after 60 secs. mixing.)

Point	x	2 arc sin $\sqrt{x}$**	$(z = \zeta_0)$ 2 [(arc sin $\sqrt{x}$) − (arc sin $\sqrt{{\cdot}5}$)†]
0, 5, A	0·851	2·3490	0·7782
1, 9, C	0·400	1·3694	− 0·2014
2, 4, B	0·385	1·3387	− 0·2321
3, 1, A	0·568	1·7072	0·1364
4, 8, C	0·428	1·4263	− 0·1445
5, 6, B	0·468	1·5068	− 0·0640
0, 6, D	0·350	1·2661	− 0·3047
1, 7, A	0·377	1·3222	− 0·2486
2, 7, B	0·422	1·4142	− 0·1566
3, 4, A	0·493	1·5568	− 0·0140

$\phi = 72{\cdot}3\,\{({\cdot}7782)^2 + ({\cdot}2014)^2 + \ldots\ldots + ({\cdot}0140)^2\} = 66{\cdot}7$

** From tables [9]. † 2 arc sin $\sqrt{{\cdot}5} = 1{\cdot}5708$.

* It can be shown that $E(\phi) = k + \lambda$

where $\lambda = \nu \sum_{i=1}^{k} (\zeta_i - \zeta_0)^2$.

When all $\zeta_i = \zeta_0$, $\lambda = 0$,

therefore when the system is completely mixed, $E(\phi) = k$.

Table 5. State of mixing after rotating the drum for various periods.

Time – secs.	$\phi = \nu \sum_{i=1}^{k} (z_i - \zeta_0)^2$
0	1541·2
20	311·7
40	124·0
60	66·7
90	36·1
120	13·7
150	14·1
180	12·2
240	7·7
300	9·0

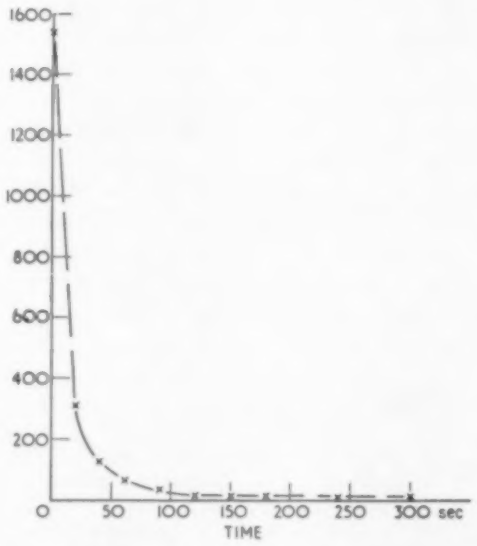

Fig. 5. Progress of mixing with time based upon values of ϕ for 10 selected.

5. Conclusions

In considering the operation of solid-solid mixing, it was considered advisable to start with a highly simplified ideal case. Thus, the distinguishing feature of all the experiments discussed in this paper is that the particles to be mixed differed only in colour. Using this ideal case as reference, the theoretical concepts of complete and incomplete mixing have been discussed and it has been concluded that the question of defining the completely mixed state is largely a statistical

one. It has been assumed that if, starting from a certain datum line, a set of mixing operations were performed and small samples were taken at various characterised points in the batch, and if this were repeated a number of times, always starting from the same datum line, then at each point, n, the number of particles in a sample and r, the number of red particles in the sample, could be represented by normal distributions. The proportion of red particles in the sample at each point may then also be represented by a normal distribution with a definite mean and variance. The definition of the completely mixed state follows as that which would obtain when the probability of drawing red at a certain point is the same at all points in the mixer. These basic assumptions have been confirmed experimentally and it has been shown, by using recognised statistical procedures, that a statistical hypothesis may be used as the test criterion for complete mixing. Furthermore, for application of this hypothesis, a comparatively limited number of samples is sufficient. In cases where the statistical criterion shows that mixing is incomplete, the progress of the mixture towards the completely mixed state may be readily followed.

It is clear that when "ideal" conditions do not hold, the problem becomes much more complicated, and may necessitate certain simplifying assumptions. However, it is considered that the method of approach and the treatment used here, as well as the conclusions reached, will serve as a sound basis for further work.

Acknowledgment

This paper is published with the permission of the South African Council for Scientific and Industrial Research.

Notation

$p(r)$ = Probability of an observation of size r.
$\binom{n}{r}$ = Binomial coefficient, ${}^nC_r$.
μ_r, μ_r' = Notation for moments about the mean and origin respectively [7].
β_1, β_2 = Coefficients of skewness and kurtosis [7].
$E(x)$ = "The expected mean value of x" [8].
$P(x > c)$ = Probability that x is greater than c.
x_k^2 = Chi-square variable with k degrees of freedom [8].
var (x) = Variance of x.
d. f. = Degrees of freedom.
$\nu = E(n)$.
θ = Probability of drawing red at a certain point.
$Z_i = 2 \arcsin \sqrt{x_i}$

References

[1] Brothman, A., Wollan, G. N. and Feldman, S. M.; Chem. and Met. Eng. 1945 **52** April 102.
[2] Coulson, J. M. and Maitra, N. K.; Industrial Chemist 1950 **26** Feb. 55.
[3] Coulson, J. M. and Maitra, N. K.; J. Imp. Coll. Chem. Eng. Soc. 1948 **4** 135.
[4] Lacey, P. M. C.; Chemical Age (Ldn.) 1945 **53** Aug. 119, 145.
[5] Buslik, D.; A.S.T.M. Bulletin No. 165 1950 (TP 92) April 66.
[6] De Jong, A. J.; Statistica 1950 **4** No. 3-4, 101.
[7] Kendall, M. G.; The Advanced Theory of Statistics, Vol. I 1948 Charles Griffin and Co. Ltd., London.
[8] Hald, A.; Statistical Theory with Engineering Applications 1952 John Wiley and Sons, N.Y.
[9] Hald, A.; Statistical Tables and Formulas, 1952, John Wiley and Sons, N.Y.

Chemical Engineering Science, 1953, Vol. 2, pp. 247 to 253. Pergamon Press Ltd.

The absorption of chlorine from air by solutions of olefins and iodine in carbon tetrachloride

G. H. Roper

School of Chemical Engineering, N.S.W. University of Technology, Broadway, Sydney, N.S.W.

(*Received* 1 *September* 1953)

Summary—The Stephens-Morris disc column is used to study the influence of chemical reaction upon the rates of absorption of chlorine from air by solutions of either cyclohexene or oleic acid with iodine in carbon tetrachloride. The increase in the liquid film coefficient due to chemical reaction between chlorine and cyclohexene was found to be independent of the concentration of cyclohexene, but no satisfactory correlation of the experimental results could be obtained.

The fractional increase in the liquid film coefficient due to reaction between chlorine and oleic acid varied from zero to 9, and was found to be

$$\phi - 1 = 39 \left[\frac{(c_C + 0{\cdot}00005)c_B}{c_i} \right] 0{\cdot}5$$

where ϕ is the ratio of the liquid film coefficient to the coefficient in the absence of reaction, c_C is the concentration of the catalyst (iodine), c_B is the concentration of oleic acid, and c_i is the concentration of the dissolved chlorine at the gas-liquid interface. The units are lb. moles, feet and hours. The film theory is unable to predict the effect of the chemical reaction on the liquid film coefficient.

Résumé—Au moyen de la colonne à disques de Stephens-Morris, l'auteur étudie l'influence d'une réaction chimique sur la vitesse d'absorption du chlore dans l'air au moyen de solutions d'iode dans CCl_4 contenant soit du cyclohexène soit de l'acide oléique.

L'accroissement du coefficient de transfert relatif au liquide accompagnant la réaction chimique entre le chlore et le cyclohexène est indépendant de la concentration de ce dernier, sans qu'il ait été possible de trouver une corrélation satisfaisante entre les divers résultats expérimentaux.

L'accroissement partiel du coefficient provenant de la réaction entre le chlore et l'acide oléique a varié entre 0 et 9 et peut être représenté par :

$$\phi - 1 = 39 \left(\frac{(c_C + 0{\cdot}00005)c_B}{c_i} \right) 0{\cdot}5$$

ou ϕ est le rapport entre les deux valeurs du coefficient avec ou sans réaction, c_C est la concentration du catalyseur (iode), c_B, la concentration de l'acide oléique, C_i, la concentration en Cl_2 dissous à l'interface gaz-liquide. Unités : lb. — moles, pieds, heures.

La théorie du film de passage ne permet pas de prédire l'effet de la réaction chimique sur le coefficient de transfert relatif au liquide.

Introduction

There has been little previous investigation on a laboratory scale into continuous absorption of a soluble gas followed by chemical reaction in the liquid. Absorption in a wetted-wall column, although continuous, does not resemble absorption in a commercial packed tower sufficiently closely to enable reliable predictions to be made of the mass transfer coefficients in the commercial tower. In a packed absorber the liquor is mixed each time it flows from one piece of packing to another. Stephens and Morris [6] designed a disc column which is suitable for small scale laboratory experiments and which gives for physical absorption results similar to those obtained in packed towers.

The disc column has been used by Stephens and Morris to study the absorption of chlorine by solutions of ferrous and ferric chlorides. With a total iron concentration equivalent to 28·7 lb. of $FeCl_3$ per cu. ft., the ratio of the ferrous chloride concentration (c_B) to the concentration

dissolved, but unreacted, chlorine at the gas-liquid interface (c_i) was varied from zero to 700. The fractional increase in the liquid film coefficient due to chemical reaction was found to be

$$\phi - 1 = 0{\cdot}75 \left[\frac{c_B}{c_i}\right]^{0{\cdot}83} \quad (1)$$

The absorption of chlorine from air by solutions 2-ethyl hexene-1 and iodine in carbon tetrachloride has been studied using a similar disc column (3). The ratio of the concentration of the olefin (c_B) to the concentration of dissolved chlorine at the interface (c_i) was varied from zero to 300. The increase in the liquid film coefficient due to chemical reaction was found to be

$$\phi - 1 = \left[\frac{bc_B}{c_i}\right]^{0{\cdot}5} \quad (2)$$

where b varied linearly with the concentration of the catalyst (iodine) and was taken to be proportional to the specific reaction rate for the addition of chlorine to 2-ethyl hexene-1 under the conditions of the absorption. In the absence of iodine, b was 0·08 and was 1·68 when the iodine concentration was 0·001 lb. moles per cu. ft.

The kinetics of the addition, in carbon tetrachloride, of chlorine to 2-ethyl hexene-1, to oleic acid, and to cyclohexene have been investigated [4]. The kinetics of the addition to 2-ethyl hexene-1 and to oleic acid may be expressed

$$\frac{dc_A}{dt} = k_a c_A c_B \quad (3)$$

where c_A and c_B refer to the concentration of the chlorine and olefin, respectively. The value of the specific reaction rate k_a, at 70°F is 155 l./(g. mol.) (sec.) or 9×10^6 cu. ft./(lb. mol.) (hr.). The kinetics of the addition to cyclohexene may be expressed

$$\frac{dc_A}{dt} = k_b c_A^2 \quad (4)$$

the reaction being second order with respect to the chlorine concentration and zero order with respect to the cyclohexene concentration when there is an excess of cyclohexene in the liquor. The value of the specific reaction rate, at 70°F, is 640 l./(g. mol.) (sec.) or 37×10^6 cu. ft./(lb. mol.) (hr.).

Experimental Procedure

The apparatus and procedure have been previously described fully [3], [6]. The absorption unit is a Stephens-Morris disc column whose major dimensions are :

Number of discs	31
Disc diameter (mean)	1·475 cm
Disc thickness (mean)	0·45 cm
Tube diameter	2·50 cm
Mean perimeter for liquid flow	0·122 ft.
Equivalent diameter for gas flow	0·052 ft.
Free space (dry)	89%
Absorption surface (dry)	0·184 ft.

The discs are threaded edgeways on a 2 mm glass rod and successive discs are maintained at right-angles.

The overall coefficients were calculated from the equation

$$K_G = N_A / A\Delta p \quad (5)$$

and were corrected for the resistance in the gas phase in order to evaluate the liquid film coefficients. The gas film coefficients were calculated from

$$\frac{k_G p_{BM}}{G_M} = 0{\cdot}15\, \Gamma^{0{\cdot}18}\, Re_G^{-0{\cdot}4}\, Sc_G^{-0{\cdot}5} \quad (6)$$

and the liquid film coefficients in the absence of a reaction from

$$Hk_L' = 0{\cdot}0041\, \Gamma^{0{\cdot}7} \quad (7)$$

For each olefin (i.e., oleic acid or cyclohexene) the first series of runs were made without using the iodine catalyst. The concentration of the physically dissolved chlorine in the liquor leaving the discs was determined from the concentration of chlorine in a hydrochloric acid solution placed in the liquor run-off tube. The total concentration of chlorine in the liquor was determined by the decrease in the olefin concentration after sufficient time had been allowed for all the chlorine to react. There was no smell of hydrogen chloride from the liquor, indicating that there was no substitution.

VOL. 2 1953

Table 1. Absorption by solutions of cyclohexene and iodine in carbon tetrachloride. Constant air rate = 0·790 c.f.m.

Run No.	Liquor								Gas % Cl_2 mean	$10^3 N_A$ liquor	K_G	Hk_L
	Rate lb./(hr.) (ft.)	Temp. °F.		$10^3 c_A$		$10^3 c_B$	$10^3 c_i$	$10^3 c_C$				
		in	out	free	total							
1	79·1	82	59	0·32	0·65	2·52	0·57	0	0·44	0·063	0·104	0·131
2	122	68	54	0·89	1·21	2·53	1·0	0	0·93	0·146	0·129	0·171
3	84·5	70	52	0·30	0·51	6·9	0·49	0	0·40	0·051	0·101	0·127
4	78·0	71	54	0·42	1·13	6·6	1·0	0	0·84	0·108	0·084	0·103
5	70·6	65	53	0·31	1·59	10·3	1·2	0	1·01	0·137	0·081	0·098
6	73·3	66	52	0·36	0·72	10·6	0·71	0	0·68	0·065	0·074	0·089
7	68·5	73	66		2·01	3·1	0·73	0·65	0·77	0·168	0·124	0·168
8	43·1	73	55		1·46	3·2	0·50	0·65	0·47	0·076	0·092	0·116
9	118	73	56		0·65	3·9	0·41	0·65	0·40	0·094	0·137	0·190
10	185	73	63		1·60	3·1	1·25	0·65	1·15	0·293	0·141	0·183

With iodine in the liquor, the presence of the interhalogen compound prevented the use of the method for determining the concentration of the physically dissolved chlorine in the liquor leaving the discs. The ratio of the physically dissolved chlorine to the total amount of chlorine absorbed was estimated from a graph in which this ratio was plotted as a function of $N_A/c_i\Gamma$ in the absence of a catalyst.

Results and Discussion

Absorption by solutions of cyclohexene

The experimental data for this absorption are given in Table 1. Six runs were made without catalyst at liquor rates from 70·6 to 122 lb./(hr.) (ft.), and four runs were made at liquor rates from 43·1 to 185 lb./(hr.) (ft.) with an iodine concentration of 0·65 × 10^{-3} lb. moles per cu. ft.

The addition of a small amount of cyclohexene to the liquor passing over the discs increased the liquid film coefficient, but further additions did not increase the liquid film coefficient (Runs 8, 6). This agrees with the kinetics expressed by equation (4) in which the rate of disappearance of chlorine is independent of the concentration of cyclohexene provided that there is sufficient olefin present to react with all the chlorine. The catalysed absorption has the same characteristics which suggests that the rate of the catalysed reaction is similarly independent of the concentration of cyclohexene.

No satisfactory correlation of the data could be obtained. Based on either the film theory or the penetration theory, an elementary treatment of absorption followed by second-order disappearance of the gaseous solute indicates that the liquid film coefficient should increase with increasing values of c_i. The data of Table 1 (runs 1, 3, 4, 5, 6 and runs 9, 10) show that c_i has the opposite effect on the coefficient. Comparable results have been obtained by Peaceman [2, p. 118] for the desorption of chlorine from water by air. He found that the film theory fails badly in explaining his experimental results. The most significant aspect of the failure is that the film theory predicts that the liquid film coefficient decreases with increasing concentration of chlorine, while it was found experimentally that the liquid film coefficient remains constant for low concentrations and then increases sharply with concentration.

Absorption by solutions of oleic acid

The experimental data for this absorption are given in Table 2. Ten runs were made without using catalyst at liquor rates from 50·2 to 241 lb./(hr.) (ft.) and seven runs were made at liquor rates from 54·5 to 118 lb./(hr.) (ft.) and with iodine concentrations from 0·09 × 10^{-3} to 0·96 × 10^{-3} lb. moles per cu. ft.

Table 2. Absorption by solutions of oleic acid and iodine in carbon tetrachloride. Constant air rate = 0·790 c.f.m.

Run No.	Liquor: Rate lb./(hr.)(ft.)	Liquor: Temp. °F. in	Liquor: Temp. °F. out	Liquor: $10^3 c_A$ free	Liquor: $10^3 c_A$ total	Liquor: $10^3 c_B$	Liquor: $10^3 c_i$	Liquor: $10^3 c_C$	Gas % Cl_2 out	Gas % Cl_2 in	$10^3 N_A$ liquor	$10^3 N_A$ gas	K_G	Hk_L
1	83·6	65	56	0·37	3·2	2·14	2·2	0	1·9	2·3	0·33	0·4	0·092	0·119
2	60·6	62	59	0·14	4·7	16·7	1·5	0	1·3	1·6	0·35	0·4	0·134	0·182
3	53·3	63	54	0·11	2·1	18·0	0·8	0	0·6	0·7	0·13	0·1	0·115	0·154
4	61·1	64	62	0·27	5·0	16·7	2·9	0	2·3	2·7	0·37	0·5	0·086	0·106
5	241	71	68	0·51	3·8	18·5	1·7	0	2·2	3·1	1·13	1·1	0·242	0·42
6	218	70	70	0·69	5·0	18·8	3·1	0	3·1	4·5	1·33	1·6	0·204	0·31
7	202	73	65	0·25	1·9	20·2	1·4	0	1·0	1·4	0·47	0·5	0·228	0·38
8	71·4	69	56	0·13	1·8	8·8	0·9	0	0·7	0·8	0·16	0·1	0·113	0·143
9	60·4	64	56	0·18	4·0	20·9	1·2	0	1·0	1·2	0·29	0·2	0·138	0·200
10	50·2	64	64	0·94	9·0	18·7	4·6	0	0·4	0·4	0·55		0·083	0·102
11	118	69	62		3·2	2·6	1·5	0·45	1·4	1·9	0·46	0·6	0·165	0·25
12	71·5	69	51		1·0	4·0	0·39	0·22	0·4	0·4	0·09		0·146	0·21
13	65·6	69	56		2·4	3·4	0·76	0·45	0·7	0·8	0·19		0·141	0·20
14	61·6	68	54		1·9	11·2	0·53	0·22	0·5	0·5	0·14		0·156	0·23
15	54·5	69	54		0·28	15·3	0·24	0·93	0·4	0·4	0·019		0·27	0·68
16	80·2	72	63		2·2	14·3	1·5	0·09	1·0	1·3	0·22		0·152	0·22
17	90·2	70	64		5·0	6·4	0·9	0·96	1·2	1·5	0·55		0·23	0·44

The film theory of gas absorption has been examined by PEACEMAN [2, pp. 206-31]. The effect of an irreversible second-order reaction of the gaseous solute with one component of the liquor is determined by two dimensionless groups : M or $k_a c_B D_A/(k_L')^2$; and q or $D_A c_i/D_B c_B$. The

Table 3. Absorption of chlorine by solutions of oleic acid.

Run No.	Γ	$10^3 c_B$	$10^3 c_i$	$10^3 c_C$	Hk_L	Hk_L'	$\sqrt{M}$	q	$\phi - 1$ expt.	$\phi - 1$ theory film	$\phi - 1$ theory pen.
1	83·6	2·1	2·2	0	0·119	0·091	1·7	2·3	0·3		0·5
2	60·6	16·7	1·5	0	0·182	0·073	6·6	0·20	1·5	3	5
3	53·3	18·0	0·8	0	0·154	0·066	7·0	0·099	1·3	4	
4	61·1	16·7	2·9	0	0·106	0·073	6·6	0·39	0·5	2	3
5	241	18·5	1·7	0	0·42	0·191	2·4	0·20	1·2		1·4
8	71·4	8·8	0·9	0	0·143	0·081	4·0	0·23	0·8		4
9	60·4	20·9	1·2	0	0·20	0·076	6·6	0·13	1·6	4	
10	50·2	18·7	4·6	0	0·102	0·064	7·4	0·55	0·6		2
11	118	2·6	1·5	0·45	0·25	0·116	4·6	1·3	1·2		0·8
12	71·5	4·0	0·39	0·22	0·21	0·080	6·2	0·22	1·6	3	5
13	65·6	3·4	0·76	0·45	0·20	0·077	8·1	0·50	1·6		2
14	61·6	11·2	0·53	0·22	0·23	0·073	11	0·11	2·2	6	9
15	54·5	15·3	0·24	0·96	0·68	0·068	28	0·035	9	17	
16	80·2	14·3	1·5	0·09	0·22	0·088	7·8	0·23	1·5	3	4
17	90·2	6·4	0·9	0·96	0·44	0·096	13	0·31	3·6	3	3

theoretical treatment of PEACEMAN is limited by the assumption that none of the gaesous solute is unreacted in the main body of the liquor. This requirement is approximated in those runs in which the concentration of the free (unreacted) chlorine in the liquor leaving the discs is small compared to the total concentration of absorbed chlorine. In Table 3 there are given the recalculated data from the runs using oleic acid in which the ratio $\phi\ (= k_L/k_L')$ is predicted by the theory to be greater than 3; the fraction of chlorine unreacted is expected to be small for these runs. The results previously published using 2-ethyl hexene-1 (3) have been similarly re-calculated and are given in Table 4. The diffusivities of the solutes, for use in calculating the dimensionless groups, were estimated by the method of ARNOLD [1]. The calculated values of the fractional increase in the liquid film coefficient ($\phi - 1$) were read from the graphical solution of PEACEMAN.

PERRY and PIGFORD [7] have published a solution for unsteady-state absorption and second-order chemical reaction (penetration theory). By assuming equal diffusivities, the effect of the chemical reaction is determined by two groups, a dimensionless time $k_g c_B t$ and c_B/c_i. For certain limiting cases, the effect of unequal diffusivities is given by replacing c_B/c_i by $D_B c_B/D_A c_i$. In evaluating ϕ from the graphs of PERRY and PIGFORD, it was assumed that the effect of D_A and D_B is the same as in the limiting cases. PEACEMAN [p. 197] has shown that the time, t, is

$$t = 4D_A/3{\cdot}14\,(k_L')^2$$

Table 4. Absorption of chlorine by solutions of 2-ethyl hexene-1

Run No.	$10^3\,c_B$	$\sqrt{M}$	$10^3\,c_i$	q	Hk_L	$10^3\,c_C$	$\phi - 1$		
							expt.	*theory*	
								film	*pen.*
2	4·7	2·5	4·9	1·9	0·116	0	0·2		0·5
3	4·8	2·5	4·6	1·7	0·125	0	0·3		0·6
4	3·9	2·3	3·1	1·4	0·125	0	0·3		0·8
5	31	6·4	0·96	0·054	0·26	0	1·7	4	2
6	30	6·3	2·2	0·124	0·147	0	0·6	4	2
7	5·1	2·6	3·4	1·1	0·146	0	0·5		0·8
8	4·2	5·3	3·2	1·3	0·158	0·20	0·5		0·8
9	5·0	5·8	2·0	0·77	0·188	0·20	1·0		1·3
10	5·8	6·2	1·1	0·33	0·25	0·20	1·6	3	3
11	7·1	6·8	0·45	0·11	0·33	0·20	2·5	4	0·9
12	9·1	11	0·19	0·037	0·83	0·30	7·7	8	3
13	6·2	9·4	1·5	0·41	0·28	0·50	2·0		3
14	5·0	8·4	2·3	0·80	0·22	0·50	1·3		1·2
15	13	19	0·53	0·073	0·61	1·04	5·5	11	14
16	34	31	0·12	0·0062	2·0	1·04	19	29	
17	32	30	0·37	0·020	1·3	1·04	13	22	
18	29	28	1·2	0·073	0·61	1·04	5·4	12	
19	27	28	2·2	0·14	0·53	1·04	4·5	7	7
20	21	12	0·10	0·0081	3·8	0·77	21	7	
21	18	11	1·2	0·12	0·92	0·77	4·6	5	2
22	12	6·9	0·75	0·11	0·67	0·42	3·1	4	9
23	11	6·6	1·4	0·22	0·55	0·42	2·4		5
24	11	2·2	2·4	0·37	0·27	0	0·6		2
26	13	2·4	0·36	0·048	0·44	0	1·9		2
27	12	6·7	2·4	0·36	0·46	0·42	1·8	3	3
28	9·5	8·0	2·5	0·46	0·56	0·77	2·4	2	2

and the other dimensionless group is thus $4k_g c_B D_A/3{\cdot}14\,(k_L')^2$, or $4M/3{\cdot}14$.

For both the film theory and the penetration theory, the calculated values of $(\phi - 1)$ are of the correct order. Both theories fail in that they predict that M is an important dimensionless group. If M were important, the correlations of the previous paper [3, Figs. 5, 6 and 7] would depend on the liquid film coefficient, k_L', and hence on the liquor rate. Similarly, the points plotted in Fig. 1 of this paper would be scattered according to liquor rate. The correlation of STEPHENS and MORRIS for the absorption of chlorine by ferrous chloride solutions similarly shows that M is not important as their correlation of $(\phi - 1)$ against c_B/c_i is independent of liquor rate.*

The reaction kinetics for the addition of chlorine to oleic acid in carbon tetrachloride are, within experimental error, the same as the kinetics for the addition to 2-ethyl hexene-1. Equation (2) for the absorption of chlorine by solutions of 2-ethyl hexene-1 and iodine in carbon tetrachloride may be re-written

$$\phi - 1 = 39\left[\frac{(c_C + 0{\cdot}00005)\,c_B}{c_i}\right]^{0{\cdot}8} \qquad (8)$$

In Fig. 1, the data from Table 1 has been plotted according to equation (8). That the data for absorption by solutions of oleic acid is in excellent agreement with the data for absorption by solutions of 2-ethyl hexene-1 is shown by the grouping of the experimental points about the solid line representing equation (8).

○ $c_C = 0$
▽ $c_C = 0{\cdot}09 \times 10^{-3}$ lb. mol/ft.^{3}
× $c_C = 0{\cdot}22 \times 10^{-3}$ lb. mol/ft.^{3}
+ $c_C = 0{\cdot}45 \times 10^{-3}$ lb. mol/ft.^{3}
△ $c_C = 0{\cdot}96 \times 10^{-3}$ lb. mol/ft.^{3}

* " In a recent paper, VAN KREVELEN and HOFTYZER [8] have reported a graphical design method for gas-liquid reactors. Their method is based on the film theory, but is inapplicable to a disc column as the group M is used. The disc column more closely resembles a commercial packed tower than does either of their experimental units, and hence their design method should be used with considerable caution for commercial towers."

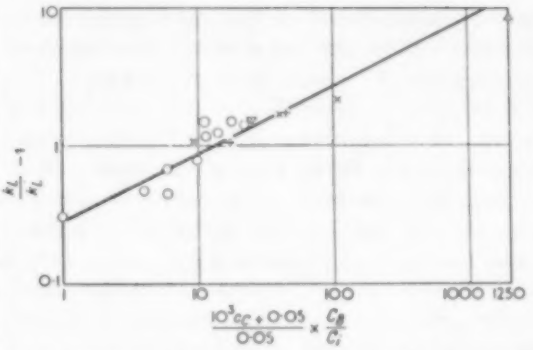

Fig. 1. The fractional increase in the liquid film coefficient due to the chemical reaction of chlorine in solutions of oleic acid and iodine in carbon tetrachloride.

CONCLUSION

The film theory has been previously criticized because it fails to predict the magnitude of the absorption coefficients in the absence of reaction, because it predicts that these coefficients are proportional to the diffusivity of the gaseous solute, and because it fails to explain the effect of concentration on the rates of desorption of chlorine from water [2], [5].

The film theory fails to explain the effect of the olefin concentration on the rates of absorption of chlorine by solutions of cyclohexene and iodine in carbon tetrachloride. The theory predicts that the fractional increase in the liquid film coefficient for the absorption of chlorine by solutions of 2-ethyl hexene-1 or oleic acid with iodine in carbon tetrachloride is affected by the liquor rate, whereas the experimental values of the fractional increase are independent of the liquor rate.

ACKNOWLEDGMENT

The author wishes to acknowledge the helpful advice received from Professor J. P. BAXTER.

NOTATION

A = surface area for mass transfer, sq. ft.
b = a parameter defined by equation (2).
c_A = concentration of chlorine, lb. moles per cu. ft.
c_B = log-mean concentration of the liquid phase reactant, lb. moles per cu. ft.
c_C = concentration of catalyst (iodine), lb. moles per cu. ft.
c_i = concentration of dissolved, but unreacted, chlorine at the gas-liquid interface, lb. moles per cu. ft.

D_A = molecular diffusivity of chlorine, sq. ft. per hr.
D_B = molecular diffusivity of liquid phase reactant, sq. ft. per hr.
G_M = mass velocity of the gas stream, lb. moles/(hr.) (sq. ft.).
H = Henry's law coefficient, lb. moles/(cu. ft.) (atm.).
k_a = specific reaction rate defined by equation (3), cu. ft./(lb. mole) (hr.).
k_b = specific reaction rate defined by equation (4), cu. ft./(lb. mole) (hr.).
k_G = gas film coefficient of mass transfer, lb. moles/(hr.) (sq. ft.) (atm.).
k_L = liquid film coefficient of mass transfer, ft. per hr.
k_L' = liquid film coefficient of mass transfer in the absence of reaction, ft. per hr.
K_G = overall coefficient of mass transfer, lb. moles/(hr.) (sq. ft.) (atm.).
M = a dimensionless group, $k_a c_B D_A/(k_L')^2$.
N_A = the rate of absorption of chlorine, lb. moles per hr.
p_{BM} = the mean partial pressure of air in the gas film, atm.
Δp = the logarithmic mean between the driving forces at each end of the column, atm.
q = a dimensionless group, $D_A c_i/D_B c_B$.
Re_G = the Reynolds' number for flow in the gas stream.
Sc_G = the Schmidt number for the gas phase.
t = time hr.
Γ = the rate of flow of the liquid layer, lb./(ft.) (hr.).
ϕ = the ratio of the liquid film coefficients $= k_L/k_L'$.

References

[1] Arnold, J. H.; J. Amer. Chem. Soc. 1930 **52** 3937.
[2] Peaceman, D. W.; Thesis in Chem. Eng., M.I.T., 1951.
[3] Roper, G. H.; Chem. Eng. Sci. 1953 **2** 18.
[4] Roper, G. H.; Chem. Eng. Sci. 1953 **2** 27.
[5] Sherwood, T. K. and Pigford, R. L.; Absorption and Extraction, 2nd ed. p. 53, McGraw Hill, New York, 1952.
[6] Stephens, E. J. and Morris, G. A.; Chem. Eng. Progress, 1951 **47** 232.
[7] Perry, R. and Pigford, R. L.; Ind. Eng. Chem., 1953 **45** 1247.
[8] Krevelen, D. W. van and Hoftyzer, P. J.; Chem. Eng. Sci., 1953 **2** 145.

Chemical Engineering Science, 1953, Vol. 2, pp. 254 to 272. Pergamon Press Ltd.

A further study of the hydraulic cyclone

D. F. KELSALL

Atomic Engergy Research Establishment, Harwell, Didcot, Berks.

(*Received* 30 *October* 1953)

Summary—By a technique involving injection of closely sized batches of *Perspex* spheres into the feed of a 3 in. hydraulic cyclone, the effect of several variables on solid elimination efficiency have been investigated.

A $\frac{1}{4}$ in. feed diameter results in maximum efficiencies on this cyclone for a wide range of conditions. It is considered impossible to derive simple power relationships to describe the effect on particle elimination efficiency of change in feed diameter, overflow diameter and throughput, to cover a range including the optimum conditions.

The importance of turbulent mixing in the feed section due to shock effects and of the short circuit flow down the outside wall of the vortex finder have been demonstrated.

Résumé—L'auteur étudie l'influence de plusieurs variables sur l'efficacité de la séparation des poussières en alimentant un cyclone hydraulique de 3 pouces avec des charges constituées de sphères en *Perspex* (plexiglas) dont les diamètres restent compris entre des limites étroites.

Pour l'alimentation de ce cyclone, un diamètre de $\frac{1}{4}$ de pouce donne une efficacité maximum dans une échelle étendue de conditions. Pour un cyclone donné, il paraît impossible de prédire l'efficacité du classement par une relation générale faisant intervenir, avec des exposants simples, chacun des facteurs : diamètre de l'alimentation et du trop-plein, débit, etc. . . pour embrasser les divers modes de fonctionnement, de par et d'autre des valeurs les plus favorables.

Ce travail souligne l'importance du mélange turbulent dans la section d'alimentation et du court-circuitage vers le bas de la paroi externe du conduit central.

1. INTRODUCTION

The extensive literature on the hydraulic cyclone contains little information about carefully controlled experiments designed to give an accurate assessment of the effect of the several cyclone variables on particle separation (or elimination) efficiencies. Most of the work reported involved the use of heterogeneous particles of various shapes and was carried out with a mixture of particle sizes under such conditions that an indeterminate amount of interference of the settling of particles in any particular size range could be exerted on particles of another size range.

Several methods of comparing efficiencies have been used. DAHLSTROM [1] uses d_{50}, the particle size in microns which reports 50% by weight to overflow and underflow. FITCH and JOHNSON [2] prefer to use a particle size which reports almost completely to the underflow (say 95%). A more reliable method involves the construction of efficiency curves which give the efficiency of elimination of the whole range of particle sizes present in the cyclone feed.

One aim of the present work was to assess the relative merits of these methods of summarising cyclone efficiencies. Another was to examine the importance of short circuiting of particles to the overflow, a phenomenon noted by the present author in a previous paper [3].

In an attempt to decrease the number of variables, pulp densities used in the present study were kept very low and throughout the testwork dilutions were effectively infinite. To eliminate the effect of shape factors and differing specific gravities of particles, almost perfect *Perspex* spheres of constant specific gravity were used.

2. EXPERIMENTAL DETAILS

Apparatus

Fig. 29a shows the cyclone to full scale. Feed openings and underflow diameters were varied by inserting interchangeable cyclone sections; vortex finders, with $\frac{1}{4}$ in. thick walls, were available such that lengths and overflow diameters were variable.

Fig. 29b provides a diagram of the apparatus.

For low pressure experiments the conical feed tank, fitted with overflow, was raised to the required height to give a constant static head. For pressures beyond the range of the head available the conical feed tank was connected to a centrifugal pump (or two in series) and the feed pressure adjusted by the setting of the valve between the pump and the pressure gauge.

Preparation of sized fractions of Perspex spheres

A miscellaneous mixture of *Perspex* spheres was closely sized by repeated wet screening in the presence of *Aerosol* OT as wetting agent. *Tyler* $4\sqrt{2}$ series screens were used down to 325 mesh. The minus 325 mesh fraction was further split into sized fractions using conventional elutriation in a multicone laboratory classifier. The classified fractions were improved by repeated sedimentasion in beakers in the presence of *Aerosol* OT until tatisfactory fractions were obtained.

Representative samples of all fractions were examined under a microscope fitted with a graduated eyepiece, several hundred grains counted and their diameters measured. The effective average diameter of each fraction was calculated as $\sqrt[3]{\frac{\Sigma N d^3}{\Sigma N}}$ and for all graphs shown in this report these average diameters were used to describe the particular fraction used for a given test.

Specific gravity determinations of samples of the various sized fractions showed that the specific gravity was 1·18 in all cases. Inclusions of air were very rare and a negligible fraction of the particles were non-spherical.

Test Procedure

The desired combination of cyclone variables was obtained by selection of the appropriate feed opening, vortex finder and underflow extension cone. The head, or pump delivery, was adjusted to give the correct operating pressure and underflow and overflow water rates were measured.

A sample of the particular batch of *Perspex* spheres, always stored under water in the presence of *Aerosol* OT to give complete wetting, was obtained by pipetting off a selected volume from the main sample, which had been well mixed by agitation, and placed in a glass separating funnel fitted with stopcock and long delivery tube. After agitation the stopcock was opened, the delivery tube filled with slurry and closed at the end with one finger. The stopcock was then closed.

The end of the delivery tube was immersed in the water in the feed cone, finger removed quickly and the tube inserted so that the open end was located in the throat of the feed funnel. The stopcock was then opened and all solids washed down with water containing *Aerosol* OT. These precautions were necessary to ensure that no air bubbles were introduced into the system.

After a time interval, found by a preliminary run with no solids but using a dye, a double deflector was moved so that the underflow and overflow streams were collected in separate containers before any solids appeared in the transparent cyclone. Collection was continued until no solids were visible within the cyclone and the deflector returned to its initial position.

The *Perspex* spheres in each container were allowed to settle under quiescent conditions for a time known to be sufficient to permit settling of all particles in the particular fraction used. The supernatant water was carefully syphoned off. The solids were washed with a minimum of water, containing wetting agent, into smaller glass containers and the procedure repeated until the underflow and overflow solids were obtained as samples containing approximately 50% water by weight in small beakers of known weight.

The final stage involved oven drying to constant weight at 80°C, followed by accurate weighing to give the weights of the dry solids.

The total weight of solids used in any test never exceeded 5 or 6 gm and the total volume of water collected often exceeded 10 litres.

3. Graphical Presentation of Results

After calculation of the percentage of the total weight of the spheres which reported to the underflow, graphs of percentage eliminated to underflow against the average particle size, measured previously, were drawn. The point corresponding to zero particle size was that given by the percentage of the total water volume flow delivered to the underflow.

A knowledge of cyclone operation leads to the conclusion that if $x\%$ is the fraction of the total water which is discharged through the underflow then, independent of any centrifugal forces acting on particles, $x\%$ of all particles must leave through the underflow. The additional percentage of particles of a given size which are discharged through the underflow is a measure of the efficiency of elimination of solids due to the cyclone action.

If $y\%$ is the experimentally determined fraction of particles of a given size eliminated via the underflow, then $(y - x)\%$ is the fraction eliminated from a total of $(100 - x)\%$ due to cyclone action. Consequently $\left(\frac{y - x}{100 - x}\right) \times 100$ is the corrected percentage of particles of a given size eliminated through the underflow as a result of centrifugal forces within the cyclone.

The graphs provided in this report show the relationship between this corrected percentage eliminated via the underflow and particle size.

Not all uncorrected curves are presented but, if necessary, they can be constructed by back

Table 1

Conditions for Series 1–6

F.D. (*ins.*)	*O.F.D.* (*ins.*)	*V.F.L.* (*ins.*)	*U.F.D.* (*ins.*)	*P* *lbs/sq. in.*	*T.F.* *litres/min.*	*U.F.* *litres/min.*	*Vol.* *% U.F.*
$\frac{3}{8}$	$\frac{1}{4}$	4	$\frac{1}{8}$	39	23·77	3·23	13·6
				18	16·80	2·47	14·7
Series 1				10	12·97	2·00	15·4
				6	10·47	1·74	16·6
$\frac{3}{8}$	$\frac{1}{4}$	4	$\frac{1}{8}$	20	13·83	1·57	11·3
				12	11·10	1·39	12·5
				8	9·34	1·29	13·8
Series 2				6	8·23	1·20	14·6
				4	6·95	1·09	15·7
				2	5·19	0·95	18·3
$\frac{1}{4}$	$\frac{3}{16}$	2	$\frac{1}{8}$	40	12·31	3·30	26·8
				20	9·34	2·63	28·2
Series 3				12	7·54	2·21	29·3
				8	6·39	1·93	30·2
$\frac{1}{4}$	$\frac{1}{4}$	2	$\frac{1}{8}$	40	15·82	1·54	9·7
				20	11·80	1·32	11·2
Series 4				12	9·57	1·18	12·3
				8	8·03	1·09	13·5
				6	7·02	1·02	14·5
$\frac{1}{4}$	$\frac{3}{16}$	2	$\frac{1}{8}$	40	18·24	0·55	3·1
				20	13·81	0·53	3·9
Series 5				12	11·01	0·53	4·8
				8	9·21	0·51	5·6
$\frac{1}{4}$	$\frac{1}{8}$	2	$\frac{1}{8}$	40	20·42	0·21	1·0
				20	15·32	0·28	1·8
Series 6				12	11·87	0·27	2·2
				8	9·86	0·27	2·7

F.D. = Feed Diameter. *O.F.D.* = Overflow Diameter. *U.F.D.* = Underflow Diameter. *V.F.L.* = Vortex Finder Length. *P.* = Pressure. *T.F.* = Total Flow. *U.F.* = Underflow.

VOL. 2 1953

calculation since in all cases the percentage water flow to the underflow is provided.

4. DETAILS OF TESTWORK

Due to the large numbers of experiments which would be necessary to undertake a complete survey of cyclone operation, selected combinations of the numerous variables were chosen in order to throw some light on the effect of the more important ones on particle elimination efficiency.

During most of the work the temperature of the water used during the experiments was not recorded, as the available information indicated that the mains water temperature was practically constant throughout the year within one or two degrees centigrade. However, experiments originally carried out during the winter months did not give the same results when repeated in the summer. In all cases the deviations could be accounted for by the increase in viscosity of water with decrease in temperature.

Most of the experiments within any one of the above sections were carried out during conditions when deviations of temperature were slight but precise comparison of the results of one section with those of another is difficult due to ambient temperature differences reaching approximately 6°C.

With very rare exceptions duplication of experimental results under exactly the same conditions was excellent. Consequently, apart from preliminary runs, no further tests were run in duplicate.

The Effect of Change in Feed Pressure Series 1 to 6

For initial experiments 4 in. long vortex finders were used but, after work had been completed which showed the effect of change in vortex finder length, it was decided to use vortex finders of 2 in. length. Consequently the first two series reported using $\frac{1}{8}$ in. and $\frac{3}{8}$ in. diameter feed openings involved 4 in. long vortex finders, $\frac{1}{4}$ in. overflow and $\frac{1}{8}$ in. underflow diameters. For the next four series 2 in. long vortex finders were used and in all four cases the feed diameter was $\frac{1}{4}$ in. but overflow diameters were $\frac{3}{16}$, $\frac{1}{4}$, $\frac{5}{16}$ and $\frac{3}{8}$ inches respectively.

Table 1 gives a summary of the conditions and water volume flows for the six series.

Figs. 1 to 6 show graphs of corrected weight percent to underflow against particle size.

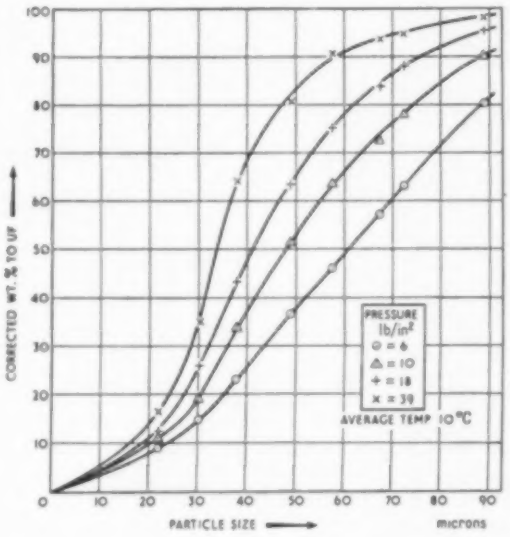

Fig. 1. Effect of feed pressure on particle elimination : Results of Series 1.

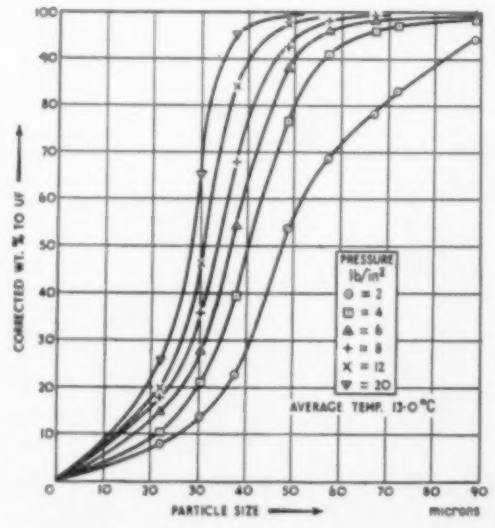

Fig. 2. Effect of feed pressure on particle elimination : Results of Series 2.

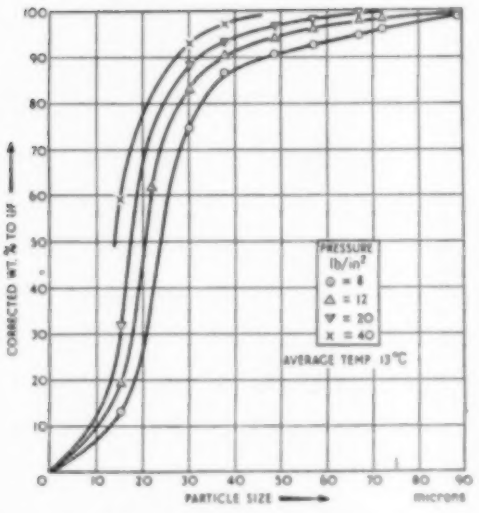

Fig. 3. Effect of feed pressure on particle elimination : Results of Series 3.

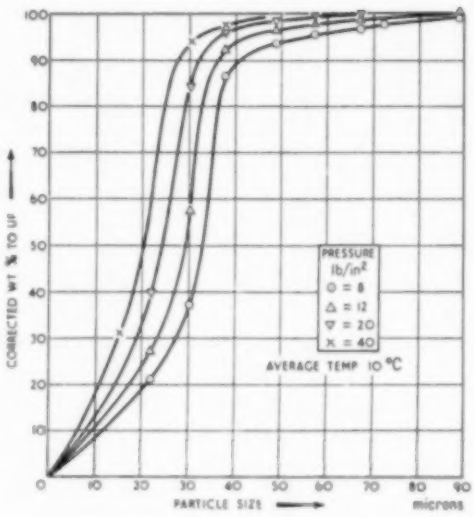

Fig. 5. Effect of feed pressure on particle elimination : Results of Series 5.

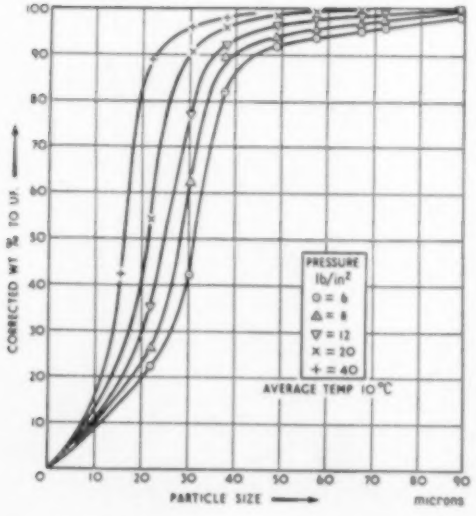

Fig. 4. Effect of feed pressure on particle elimination : Results of Series 4.

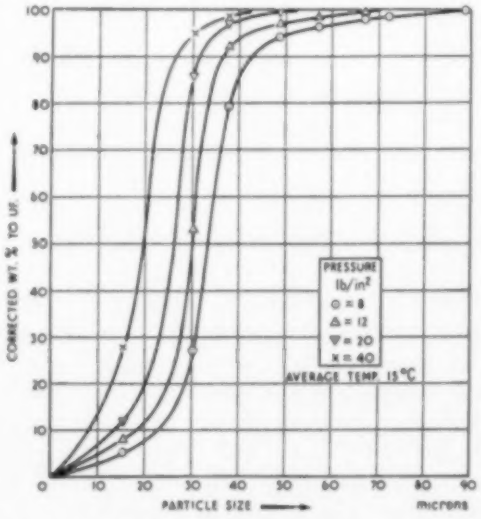

Fig. 6. Effect of feed pressure on particle elimination : Results of Series 6.

VOL. 2 1953

Fig. 7 gives the relationship between d_{50} and feed pressure, and Fig. 8 between total throughput (G) and feed pressure. (In constructing Fig. 7 small corrections were made for changes in water viscosity with temperature. On the assumption that STOKES' Law governs the settling rates, $d_{50} \propto \sqrt{\mu}$ where μ = viscosity.)

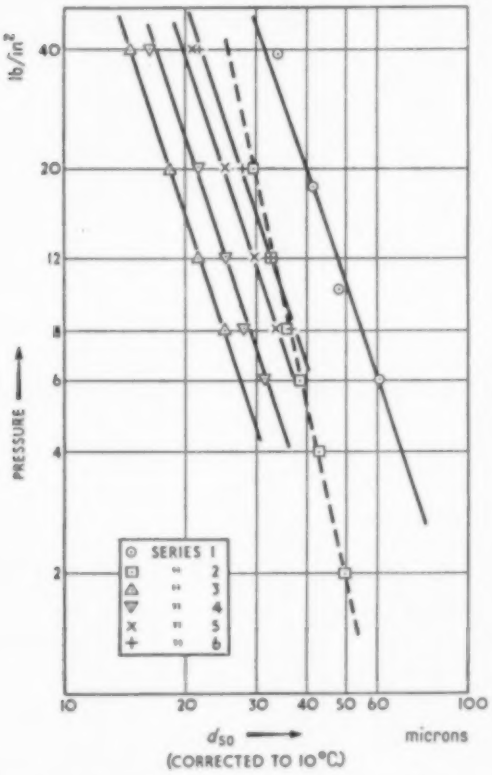

Fig. 7. Relationship between feed pressures and d_{50} values: Series 1–6.

Fig. 7 shows that for series 1, 3, 4, 5, and 6

$$P \propto \frac{1}{d_{50}^{3}}$$ and for series 2

$$P \propto \frac{1}{d_{50}^{4 \cdot 52}}$$

From Fig. 8 it can be seen that for all series $G \propto P^{0 \cdot 416}$ or $P \propto G^{2 \cdot 4}$.

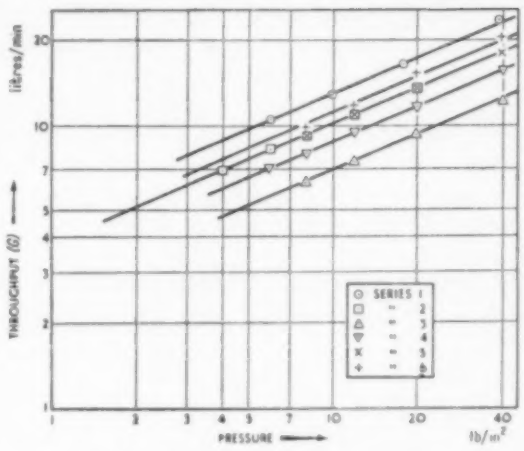

Fig. 8. Relationship between feed pressure and total throughput : Series 1–6.

Hence for series, 1, 3, 4, 5 and 6

$$d_{50} \propto \frac{1}{G^{0 \cdot 80}}$$ and for series 2

$$d_{50} \propto \frac{1}{G^{0 \cdot 58}}$$

Further experiments are needed to throw more light on this phenomenon but it may be concluded that for any given combination of cyclone dimensions there exists a simple power relationship between feed pressure, or throughput, and d_{50}, and that the limited results indicate that the power is not constant.

The Effect of Change in Feed Diameter and Shape of Feed Opening

The Effect of Change in Feed Diameter

For the first series feed pressure was maintained constant at 6 lbs./sq. in., overflow diameter $\frac{1}{4}$ in., vortex finder length 4 in. and underflow diameter $\frac{1}{8}$ in. Selected particle sizes were passed through the cyclone for a range of feed diameters.

The second series was a repetition of the first but with a constant feed pressure of 15 lbs./sq. in.

For the third series the length of the vortex finder was decreased to 2 in. but all other variables were maintained as for series 2.

The fourth series involved two sets of conditions selected at random to give wide changes in overflow and underflow diameters.

The fifth series involved a repetition of series 2 and 3 but using vortex finders $\frac{1}{8}$ in. in length. A further test was made in which no vortex finder was used, the overflow being a circular hole in the top of the cyclone (i.e. zero length vortex finder).

Figs. 9, 10, 11, 12 and 13 summarize the results of the respective series.

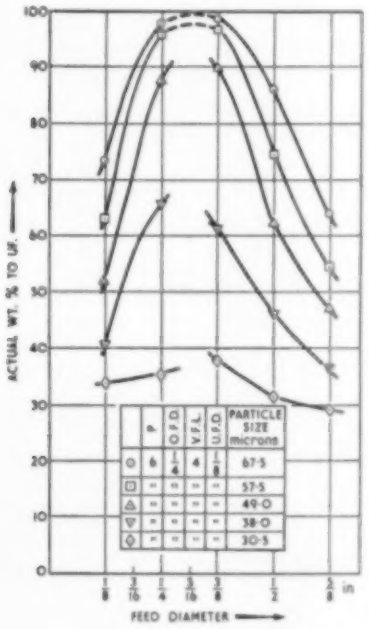

Fig. 9. Effect of change in feed diameter : first series.

The weight per cents graphed are those obtained by experiment and are uncorrected. No significant alteration of the shape of the curves was obtained using corrected results. Consequently, for convenience, actual results were used.

Inspection of Figs. 9 to 13 reveals that, without exception, for a wide range of conditions, an optimum feed diameter exists with an approximate value of $\frac{1}{4}$ in. to $\frac{5}{16}$ in.

Figs. 9, 10 and 11 show the marked increase in efficiency for all particle sizes as the feed diameter decreases from $\frac{3}{8}$ in. to $\frac{1}{4}$ in.

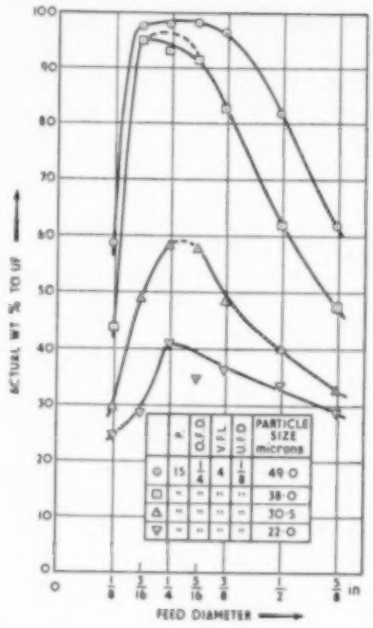

Fig. 10. Effect of change in feed diameter : second series.

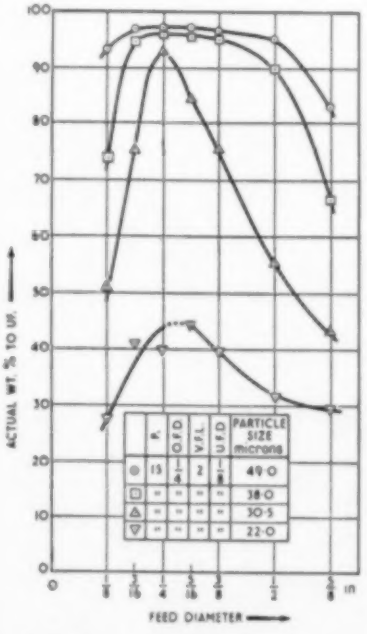

Fig. 11. Effect of change in feed diameter : third series.

VOL. 2 1953

Fig. 12, the results of conditions selected at random, shows that within the accuracy of the experiments, a feed opening of $\frac{1}{4}$ in. diameter gives optimum particle elimination for overflow diameters of $\frac{1}{2}$ in. and $\frac{1}{8}$ in.

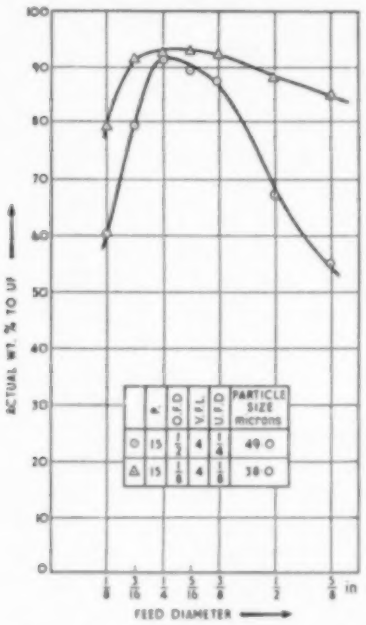

Fig. 12. Effect of change in feed diameter : fourth series.

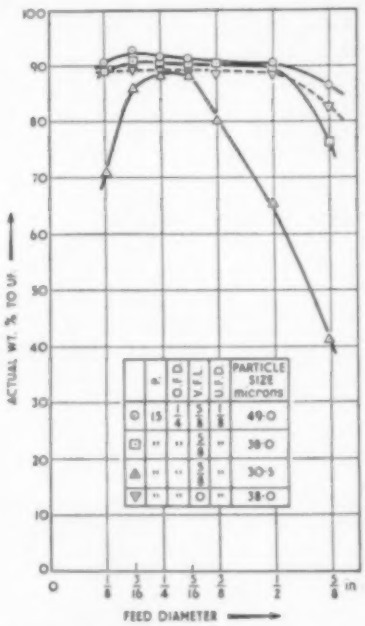

Fig. 13. Effect of change in feed diameter : fifth series.

No further experiments were undertaken but it is inferred that, for all practical purposes when using a 3 in. cyclone, optimum elimination of all particles is obtained using a feed diameter of $\frac{1}{4}$ in. to $\frac{5}{16}$ in.

Additional conclusions may be drawn from a consideration of the curves for 49 microns particles in Figs. 10, 11 and 13, which throw considerable light on the effect of vortex finder length on the efficiency of elimination of relatively coarse particles. However, this aspect is dealt with later.

The Effect of Change in Feed Diameter on the Rate of Injection of Momentum

In view of the interesting results given in the previous section a detailed study was made of total volume flows (through-puts, G) for a wide range of cyclone conditions. The procedure involved selection of a given feed pressure, overflow diameter and underflow diameter and measurement of total flows for a range of feed diameters. The vortex finder length was maintained constant at 4 in.

Average feed velocities (V_{AV}) were calculated and graphs of V_{AV} against feed diameter constructed. By interpolation from the graphs it was possible to calculate accurate values of $G\,V_{AV}$ for each set of cyclone conditions. Graphs were then drawn showing the relationship between $G\,V_{AV}$ and feed diameter, with all other cyclone variables constant for each curve.

Fig. 14, which is confirmed by many similar figures not presented in this report, shows that for any given set of cyclone dimensions and feed pressure there exists a feed diameter which gives a maximum value of $G\,V_{AV}$ and that this feed diameter is independent of feed pressure.

Fig. 15 shows that a very simple linear relationship exists between this optimum feed diameter and the overflow diameter.

Since G is the volume (or mass) rate of addition of water to the cyclone, it follows that $G\,V_{AV}$ is a measure of the rate of injection of momentum

into the cyclone i.e. momentum added per unit time. It appears therefore, that for any selected feed pressure and combination of cyclone dimensions, there is a feed diameter (D_f) which results in an optimum rate of injection of momentum, and that its value bears a simple relationship to the diameter of the overflow orifice. Within the limits of accuracy of the experiments, D_f is independent of the actual value of the feed pressure and also independent of the underflow diameter.

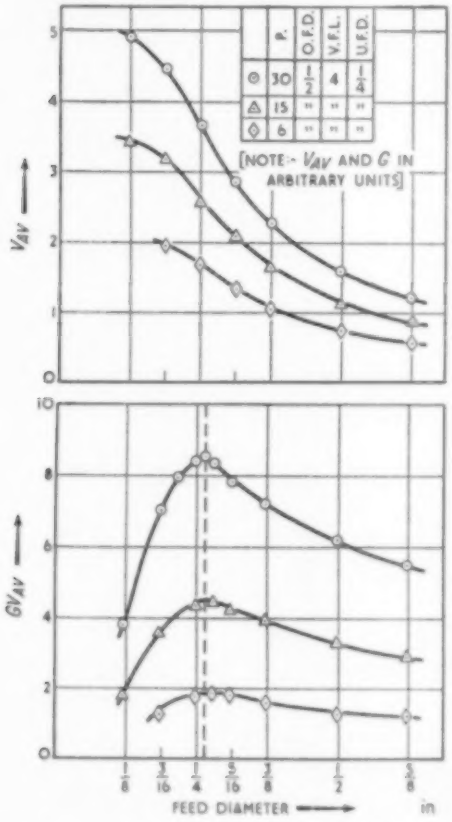

Fig. 14. Average feed velocities against feed diameter and calculated $G\,V_{AV}$ values against feed diameter.

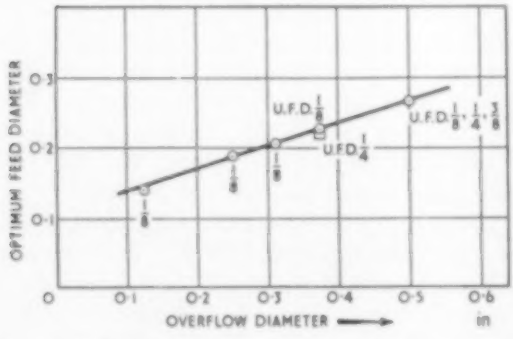

Fig. 15. Relationship between optimum feed and overflow diameters.

In unpublished data available to the author, and relating to dust extraction cyclones, reference has been made to the fact that the average velocity of entry of gases into cyclones can vary from a fraction of, to several times, the tangential velocity of the gas at the same radius.

In addition it has been found that maximum particle elimination efficiency is obtained when the two velocities are approximately equal. Assuming that the same phenomenon exists with hydraulic cyclones and, taking into consideration the fact that envelopes of constant tangential velocity in the conical portion of a hydraulic cyclone are concentric cylinders [3], it is highly probable that D_f is that feed diameter which results in the average velocity at the average feed radius (measured from the axis of the cyclone) being approximately the same as the tangential velocity at the same radius.

Under these conditions the difference between the average velocity of the new feed water and the velocity of the water already rotating within the cyclone at the same radius would be small and the resultant turbulent mixing would be at a minimum. Similarly the rate at which momentum would be "wasted" in producing undesirable turbulence would also be a minimum.

Such turbulent mixing of the water in the feed portion of a cyclone must also result in a similar mixing of the solid particles present in the cyclone feed.

The Effect of Change in Shape of the Feed Opening

Two main reasons offered possible explanations of the effect of change in feed diameter on particle elimination efficiency (all other variables kept constant) :

(*a*) The effect of turbulent mixing in the feed section of the cyclone as described above.

VOL. 2 1953

Table 2

Comparison of volume flows for circular and rectangular feed openings

Rectangular		Circular	Area	Total flows		Underflows		% U.F.	
Length	Width	Diameter	Sq. ins.	Rect.	Circular	Rect.	Circular	Rect.	Circular
·818″	$\frac{3}{8}$″	$\frac{1}{2}$″	·307	14·87	15·74	2·12	2·29	14·3	14·5
·785″	$\frac{1}{4}$″	$\frac{1}{2}$″	·196	13·76	14·07	1·83	1·92	13·3	13·7
·590″	$\frac{3}{16}$″	$\frac{3}{8}$″	·110	12·38	12·45	1·54	1·56	12·5	12·5
·393″	$\frac{1}{8}$″	$\frac{1}{4}$″	·049	10·29	10·36	1·16	1·18	11·3	11·4

(*b*) The fact that all particles did not enter the cyclone at exactly the same radius. With large feed openings some particles must enter at appreciably smaller radii than others and have a greater distance to settle outwards into the vertical downward flows which reject them to the underflow.

In order to investigate (*b*) rectangular feed openings were constructed which had the same area as selected circular feed openings. The rectangular side parallel to the axis of the cyclone was kept as large as possible so that the side parallel to any radius of the cyclone was short. Duplicate standard tests were carried out using solids injected into the feed with circular and equivalent area rectangular feed openings.

In all cases the feed pressures were kept constant at 15 lbs./sq. in. or 6 lbs./sq. in. Vortex finders were 2 in. long and overflow diameters $\frac{1}{4}$ in. Underflow diameters were $\frac{1}{8}$ in. in all cases.

Both Figs. 16 and 17 indicate that rectangular feed openings give slightly improved efficiencies for all particle sizes, and that the improvement

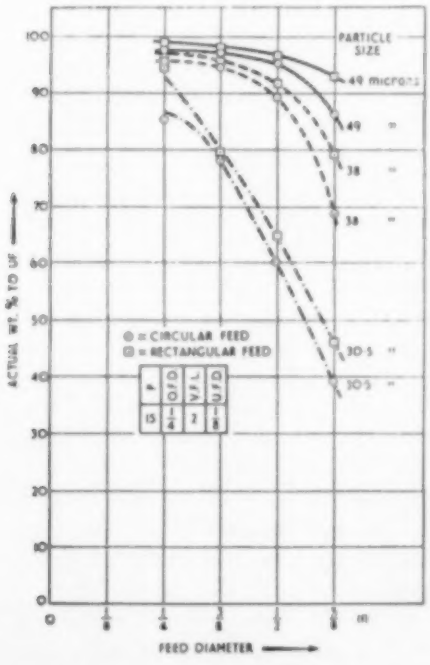

Fig. 16. Effect of shape of feed inlet on weight discharged to underflow.

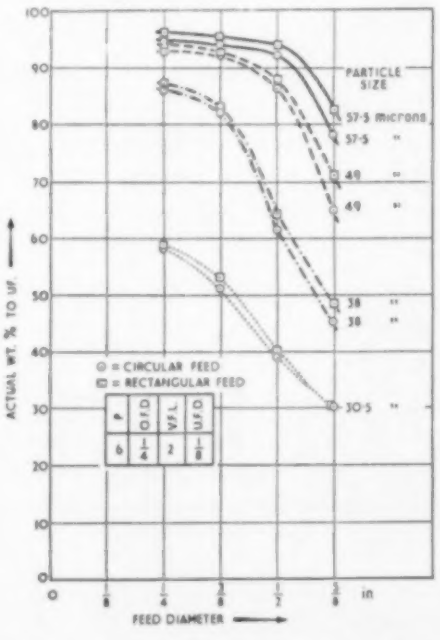

Fig. 17. Effect of shape of feed inlet on weight discharged to underflow.

is greatest for the largest feed openings for the same feed pressure. Volume flows are slightly decreased by changing to rectangular feeds.

Crude Pressure Drop Studies

Using a vortex finder 4 in. long, overflow diameter $\frac{1}{4}$ in. and underflow diameter $\frac{1}{8}$ in., total volume flows were measured at a pressure of 15 lbs./sq. in. for a range of feed diameters.

In turn the feed jets were unscrewed from the cyclone and measurements made of the feed pressures necessary to give the same total volume flows as those obtained with the various feed jets when installed in the cyclone. The pipe line and position of the pressure gauge were unchanged.

Under these conditions the average water velocities in the pipe line and through the jets were the same with and without the cyclone connected. Consequently friction losses were the same and the difference between the two pressures for each feed jet gave a measure of the pressure drop *within the cyclone* during normal operation.

In Fig. 18 the results are expressed as the fraction of the total feed pressure which was "dropped" within the cyclone graphed against feed diameter.

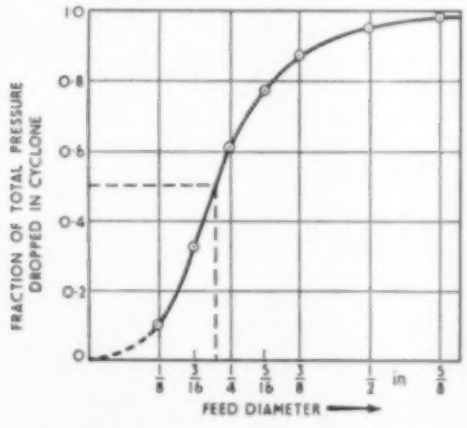

Fig. 18. Fraction of feed pressure dropped in the cyclone against feed diameter.

The results indicate that with large feed openings a major fraction of the pressure drop occurs within the cyclone. This can be explained as suggested previously by the excessive turbulence which is caused in the feed section of the cyclone. For small feed openings the greater fraction of the pressure drop occurs in the feed pipe from the pressure gauge to the point of entry into the cyclone.

Optimum particle elimination efficiency is obtained when approximately 50% of the total pressure drop occurs within the cyclone.

Conclusions

(1) Using a 3 in. cyclone and a wide range of conditions it appears that a $\frac{1}{4}$ in. feed diameter gives optimum solid elimination efficiency for all particle sizes.

(2) To a first approximation optimum solid elimination efficiency is obtained under conditions which result in the maximum rate of injection of momentum for a given feed pressure.

(3) Long, narrow rectangular feed openings give slightly improved efficiencies when compared with circular openings of the same cross sectional areas.

(4) It is highly probable that with hydraulic cyclones smaller or greater than the 3 in. size used in this study, the conditions required to give maximum solid elimination efficiencies can be obtained by volume flow measurements to determine the conditions necessary for maximum rate of injection of momentum.

(5) It is of interest to compare the rough economics of inefficient solid elimination using a $\frac{3}{8}$ in. feed with the highly efficient elimination obtained using a $\frac{1}{4}$ in. feed.

Taking the results given in Table 2 as typical examples and remembering that, for the same feed pressure and identical cyclone dimensions, the $\frac{1}{4}$ in. feed gives solid elimination efficiencies which are considerably greater than those given by a $\frac{3}{8}$ in. feed (Figs. 9, 10, 11, 12 and 13), it will be seen that, in spite of the fact that the feed area of the $\frac{1}{4}$ in. opening is only approximately one sixth of the $\frac{3}{8}$ in. feed, the total flow is 10·36 litres/min. compared with 15·74.

Consequently three cyclones with $\frac{1}{4}$ in. feeds will treat the same total volume as two cyclones, of the same size, with $\frac{3}{8}$ in. feeds operating at the same feed pressure.

VOL. 2 1953

Pumping costs may be regarded as a direct function of the volume handled and will be almost identical. For the additional cost of a cheap cyclone assembly the same total volume can be treated with greatly improved solid elimination efficiency.

The Effect of Change in Overflow Diameter

Four series of experiments were carried out. Particle elimination efficiencies were measured using the standard technique.

In the first series, at a feed pressure of 6 lbs./sq. in., a $\frac{1}{2}$ in. feed diameter and $\frac{1}{8}$ in. underflow diameter were used. Vortex finders were 4 in. long and overflow diameters of $\frac{1}{8}$, $\frac{3}{16}$, $\frac{1}{4}$, $\frac{5}{16}$, $\frac{3}{8}$ inches were used.

The second series was carried out under the same conditions except that the feed diameter was $\frac{3}{8}$ in.

For the third and fourth series feed diameters were $\frac{1}{4}$ in. (shown to give optimum efficiencies), underflow diameters $\frac{1}{8}$ in. and all vortex finders were 2 in. long. The conditions for the fourth series were the same as for the third except that the feed pressure was increased from 8 lbs./sq. in. to 20 lbs./sq. in.

Figs. 19, 20, 21 and 22 summarize the results graphically. Corrected weight per cents to underflow were calculated and used for the graphs.

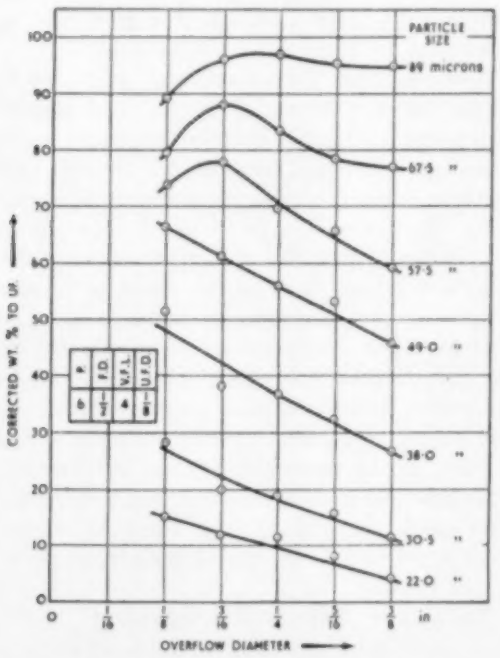

Fig. 19. Effect of change in overflow diameter : first series.

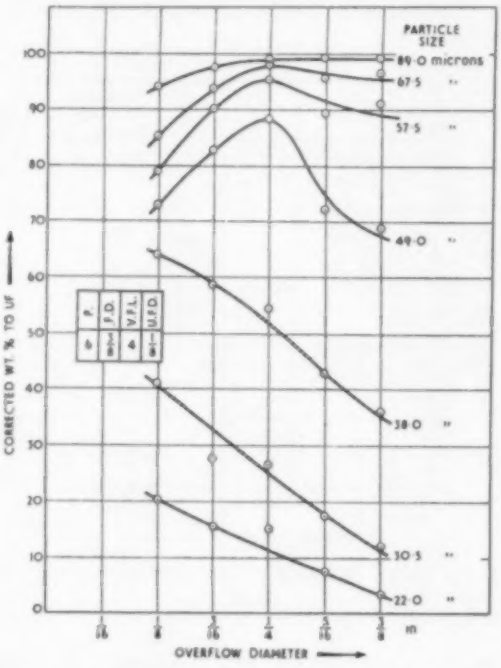

Fig. 20. Effect of change in overflow diameter : second series.

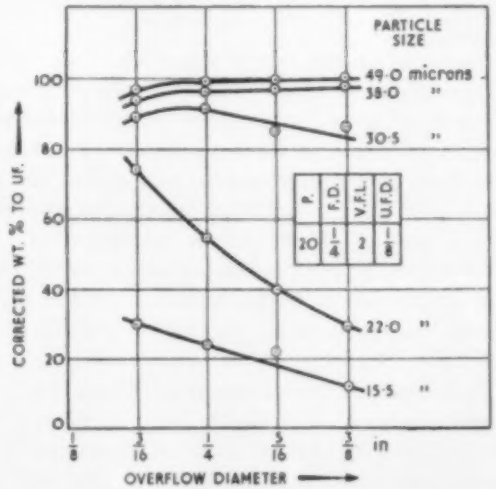

Fig. 21. Effect of change in overflow diameter : third series

As the overflow diameter is decreased the efficiency of elimination of the finer sizes increases steadily but the coarser sizes behave differently in that the efficiency increases to a maximum and then decreases (appreciably under some conditions) with further decrease in overflow diameter.

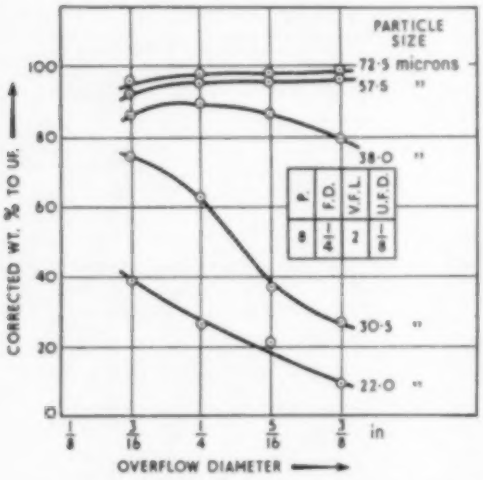

Fig. 22. Effect of change in overflow diameter : fourth series.

For a $\frac{1}{2}$ in. feed, a $\frac{3}{16}$ in. overflow gives the maximum efficiency (all other cyclone variables kept constant). For $\frac{3}{8}$ in. and $\frac{1}{4}$ in. feed diameters the optimum overflow diameter is approximately $\frac{1}{4}$ in.

Anticipating the results reported in the next section it is considered that this fall off in efficiency of the elimination of the coarser sizes with further decrease in overflow diameter is a direct result of the short circuit flow down the outside wall of the vortex finder. Referring to a previous paper by the author [3] it will be recalled that the short circuit flow turns sharply along the bottom face of the vortex finder wall to join the main overflow stream and results in high inward radial velocities.

In the same paper it was pointed out that, for a wide range of conditions, the maximum tangential velocity was attained at approximately 0·2 in. from the axis of the cyclone. The position of this maximum was *independent of the overflow diameter*, and from this position to the air/water interface the tangential velocity decreased as radius decreased according to the relationship $V \propto r$.

The centrifugal acceleration $\frac{V^2}{r}$ therefore tends to vary directly as r. This relationship holds for all horizontal levels beneath the bottom of the vortex finder, including the position in very close proximity to the bottom face of the vortex finder, i.e. in the region where the short circuit flow turns beneath the bottom of the vortex finder.

For radii greater than 0·2 in. the relationship Vr^n held and consequently $\frac{V^2}{r}$ increased with decrease in radius.

With large overflow diameters, such that the overflow radius plus vortex finder wall thickness (0·125 in.), i.e. the radius of the outside wall of the vortex finder, is greater than 0·2 in., any decrease in overflow diameter for constant wall thickness results in solid particles in the short circuit flow having to pass through regions in which the centrifugal acceleration is greater. Consequently more particles of a given size are eliminated from the short circuit flow.

However, once the outside wall radius of the vortex finder is decreased to less than approximately 0·2 in., further decrease results in regions of smaller centrifugal accelerations through which particles carried by the short circuit flow must pass. This results in progressively less efficient elimination of particles of a given size carried by the short circuit flow, as the overflow diameter is decreased. (Constant wall thickness assumed.)

It has been demonstrated previously [3] that the short circuit flow along the outside wall of the vortex finder occurs in a region of poor solid elimination efficiency. Therefore, only a small fraction of the finer particles can be eliminated from this flow and, in any case, most of the finer sizes discharged through the overflow originate from regions in the bottom of the conical portion of the cyclone.

The gain in efficiency of elimination of the main fraction of particles in a given fine size range, due to the decrease in overflow diameter, will mask

VOL. 2 1953

the decrease in efficiency of elimination of the same particles from the short circuit flow.

Practically all the coarse particles discharged through the overflow are due to the short circuit flow and consequently, as the efficiency of elimination from the short circuit flow decreases as the overflow diameter is decreased beyond the optimum size, then the percentage of such particles discharged through the underflow decreases and the overall efficiency for these particles also decreases.

The Effect of Change in Vortex Finder Length

Three series of experiments were carried out in which the length of the vortex finder was varied from $\frac{1}{8}$ in., to 2 in. to 4 in., measured from the top of the cyclone.

The conditions were :

1st Series : 6 lbs./sq. in., $\frac{3}{8}$ in. feed diameter, $\frac{1}{4}$ in. overflow diameter, $\frac{1}{8}$ in. underflow diameter.

2nd Series : 15 lb./sq. in., $\frac{1}{4}$ in. feed, $\frac{1}{4}$ in. overflow, $\frac{1}{8}$ in. underflow.

3rd Series : 15 lb./sq. in., $\frac{3}{8}$ in. feed, $\frac{1}{4}$ in. overflow, $\frac{1}{8}$ in. underflow.

Inspection of Figs. 23, 24 and 25 shows that an increase in efficiency is obtained for the finer sizes (i.e. the lower settling rate particles) as the length of the vortex finder is decreased.

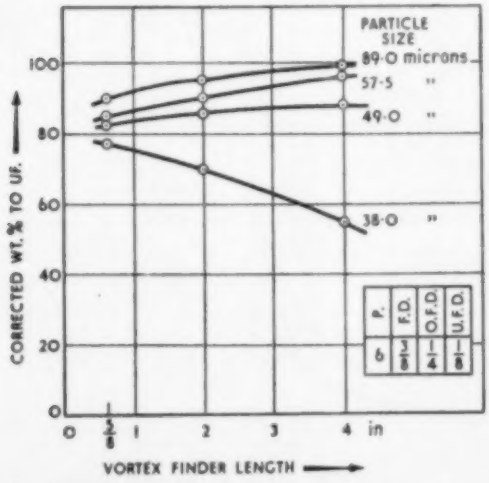

Fig. 23. Effect of vortex finder length : first series.

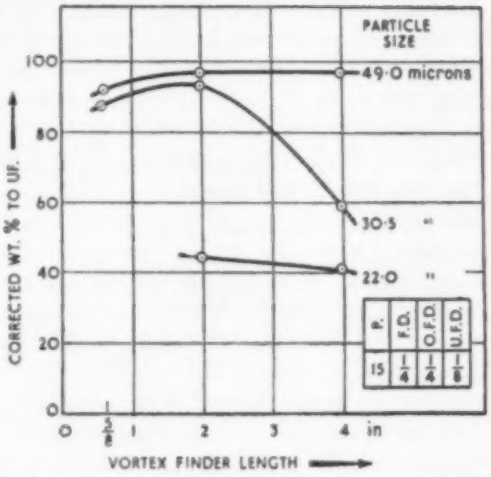

Fig. 24. Effect of vortex finder length : second series.

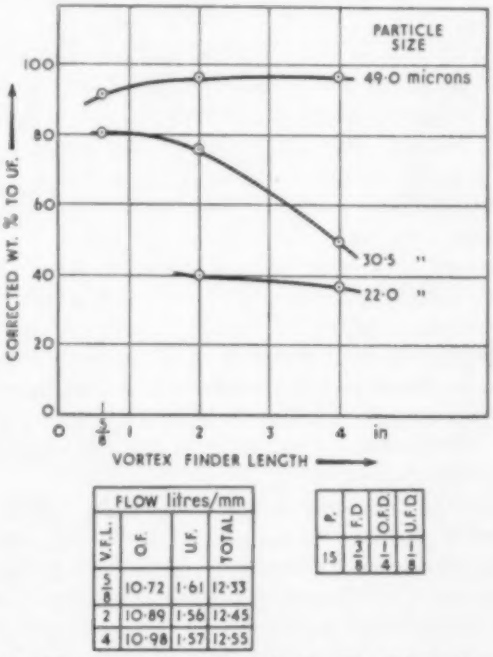

V.F.L.	FLOW litres/mm O.F.	U.F.	TOTAL
5/8	10·72	1·61	12·33
2	10·89	1·56	12·45
4	10·98	1·57	12·55

Fig. 25. Effect of vortex finder length : third series.

The efficiency of elimination of coarsest sizes decreases noticeably, up to 10% in some cases, with decrease in vortex finder length.

Fig. 24 indicates that for some particles the efficiency increases to a maximum and then decreases with further reduction in length of vortex finder.

The table of flow rates provided with Fig. 25, as a typical example, shows that these changes in efficiency cannot be attributed to changes in throughput or the slight changes in overflow flow rate.

Relatively simple explanations are possible.

The majority of the particles in the finer size ranges which are discharged through the overflow have passed down the cyclone outside the zero vertical velocity envelope [3] and, in the lower regions of the cyclone, have been carried inwards by the water radial velocity components to join the high velocity upward flows near the central air column. As the radial velocities at any radius tend to decrease as the bottom of the vortex finder is approached, whereas the centrifugal acceleration at the same radius remains unchanged, such particles tend to move outwards again.

With a short vortex finder the time available for them to leave the vertical flows, which eventually reach the vortex finder direct, is much greater than when a long vortex finder is used. (It is considered that velocity profiles below the bottom of the vortex finder are not appreciably changed by the length of the vortex finder.) Consequently a greater fraction of the particles may join the recirculation [3] to the feed section of the cyclone, where mixing occurs, and may make repeated passes through the main cyclone flows. The expected overall result is that shorter vortex finders will lead to higher efficiencies for the finer sizes. This result is demonstrated in Figs. 23, 24 and 25.

If the assumption that practically all the coarser particles discharged through the overflow originate from the short circuit flow is correct, increase in the length of the vortex finder would permit a longer time interval for such particles to be slowly eliminated from the short circuit flow, and, if the same or similar velocity profiles are sustained within the short circuit flow for the whole length of the vortex finder, the overall result would be a higher efficiency of elimination through the underflow, since particles leaving the short circuit would be redistributed within the feed section and a major fraction would enter the main downward flows within the cyclone.

The Effect of Change in Underflow Diameter

Since in practical cyclone operation the main factor governing the selection of the underflow diameter is the quantity of solids to be discharged through this orifice, and the total time available for the whole investigation had to be limited, only two tests were carried out.

For both tests pressures were maintained at 6 lbs./sq. in. In the first a $\frac{1}{8}$ in. feed was used with $\frac{3}{8}$ in. overflow diameter and 4 in. long vortex finder. Underflow diameters were $\frac{1}{4}$ in. and $\frac{1}{8}$ in.

The second test involved use of a $\frac{3}{8}$ in. feed and other conditions were the same as for the first test.

Table 3

Flow Rates

Underflow diam.	$\frac{1}{8}$″ *feed (litres/min.)*			$\frac{3}{8}$″ *feed*		
	O.F.	*U.F.*	*Total*	*O.F.*	*U.F.*	*Total*
$\frac{1}{4}$″	12·56	4·36	16·92	9·61	2·97	12·58
$\frac{1}{8}$″	13·43	0·56	15·99	11·43	0·28	11·71

Fig. 26 summarizes the results.

Under the conditions of the experiments, i.e. constant feed pressure and very low pulp densities,

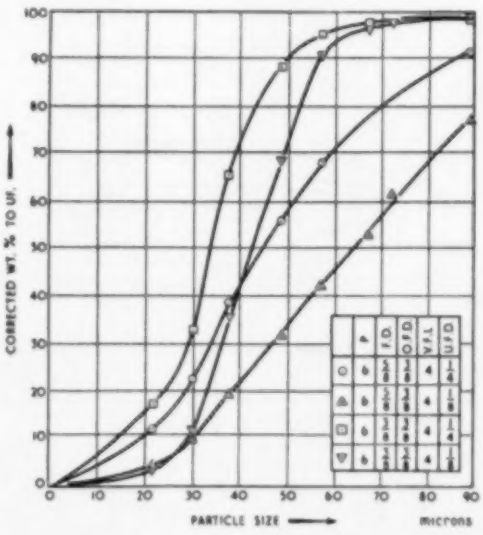

Fig. 26. Particle elimination for different underflow diameters.

VOL. 2 1953

it is seen that decrease in underflow diameter results in a decrease in efficiency of elimination of particles of all sizes.

Table 4 shows that with small underflows the volume flowrate through the overflow increases appreciably but that total flows are only slightly changed.

It can be postulated from a general knowledge of velocity profiles within the cyclone [3] that under the above experimental conditions tangential velocity profiles would be very similar but radial and vertical velocities in regions beneath the bottom of the vortex finder would be appreciably greater when using smaller underflow diameters. Consequently, coarser particles would tend to be discharged through the overflow in larger quantities. However, much testwork is needed to confirm or disprove this crude theory.

Annulus Experiments

In order to obtain a quantitative assessment of the value of the modification (U.K. Patent Application No. 1358/52), described in a previous paper [3], for diminishing the effect of the short circuit flow, a simple experiment was undertaken.

The cyclone was set up with a $\frac{3}{8}$ in. feed, $\frac{1}{8}$ in. underflow and $\frac{1}{4}$ in. overflow. The vortex finder was 2 in. long and had a wall $\frac{1}{8}$ in. thick. An annular take off was incorporated around the root of the vortex finder, in the flat top of the cyclone, with a diameter of $\frac{13}{16}$ in. The construction was such that a separate discharge could be taken off through the $\frac{5}{32}$ in. wide annulus by a pipe fitted with a valve.

Table 4

Flow rates for Annulus Test

Pressure lbs./sq. in.	*litres/min.*		
	Overflow	*Annulus*	*Underflow*
5·9	5·63	3·61	0·83

Feed pressure was kept constant at 5·9 lb./sq. in., and by adjustment of the valve a suitable fraction of the total flow was taken through the annulus. The usual procedure with batches of sized *Perspex* spheres was adopted but, in this case, particles discharged by the overflow, annulus and underflow were all collected separately for drying and weighing.

In Fig. 27 the actual weight percents discharged through the respective openings are graphed against particle size.

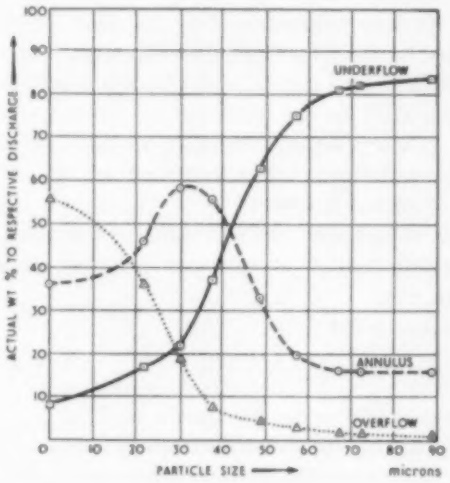

Fig. 27. Elimination of particles through overflow, underflow and annulus.

For the coarser sizes the weight per cent discharged through the annulus tends to a limiting value of approximately 15%. As it is virtually impossible for very coarse particles to reach the annulus from the lower regions of the cyclone, it is considered that this phenomenon indicates that, of the water discharged through the annulus, an amount equal to 15% of the total water flow through the cyclone is short circuited directly from the feed to the annulus and that, for all solids independent of size, a fraction equal to 15% of the solids in the feed is short circuited from the feed to the annulus.

In order to obtain some information about the fraction of all solids discharged through the annulus *but originating from the lower regions of the cyclone*, and carried to regions above the bottom of the vortex finder by the recirculation to which reference has already been made, the actual weight per cents discharged through the

three openings were corrected in the following manner.

Let $x\%$ of the total volume flow pass through the underflow. Then by a previous argument (Section 3) (100-x) is the corrected feed and $(y - x)$ is the fraction eliminated through the underflow by the cyclone action ($y\%$ is the experimentally determined fraction eliminated through the underflow).

A further correction for the feed solids is needed for the 15% short circuit i.e. $(100 - x - 15)$ is the final feed corrected for both underflow and short circuit to the annulus.

If z is the actual weight % of selected solids discharged through the annulus then $(z - 15)$ is the corrected fraction.

On this basis, with double correction, the corrected weight per cent to the underflow is $\frac{(y - x)}{(100 - x - 15)} \times 100$, the corrected weight per cent to the annulus $\frac{(z - 15)}{(100 - x - 15)} \times 100$ and the remainder to the overflow.

Fig. 28 is of considerable interest. Remembering that the short circuit direct from the feed has been eliminated mathematically by the above corrections, inspection shows that the coarse particles have a very high probability of discharge through the underflow as a result of cyclone action, but very low probabilities of discharge through the overflow or the annulus.

Very fine particles have a high probability of discharge through the overflow but low probabilities of discharge through the underflow or annulus.

Under the conditions of the experiment particles of intermediate size (i.e. in the region of 30 microns) have low probabilities of discharge through either the overflow or the underflow. They have, however, a relatively high probability of discharge through the annulus.

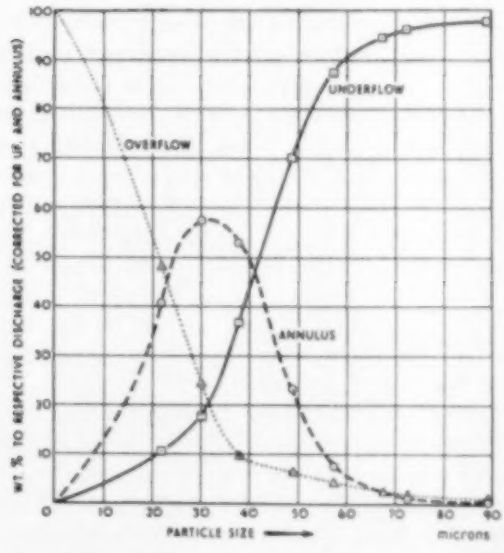

Fig. 28. Particle elimination through overflow, underflow and annulus corrected for annulus and underflow factors.

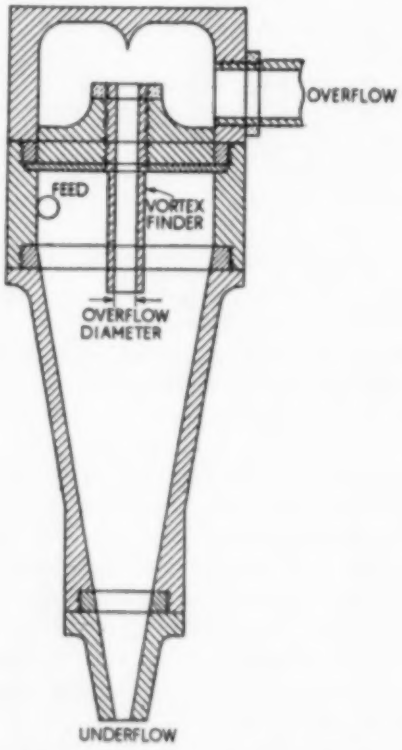

Fig. 29a. Vertical section through cyclone showing construction

Flow patterns within the cyclone must be affected by withdrawal of a portion of the flow through the annulus, but it is considered highly probable that the result presented in Fig. 28 provides a *qualitative* picture of the behaviour of

intermediate particles during normal cyclone operation. As confirmation it may be stated that during the extensive testwork described in this report it was often noted that some particles required excessively long periods of time before they were completely eliminated from the cyclone, and the recirculation, already described, was easily visible in regions above the bottom of the vortex finder.

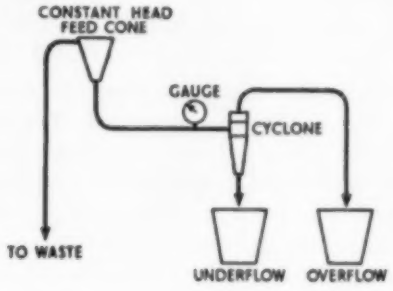

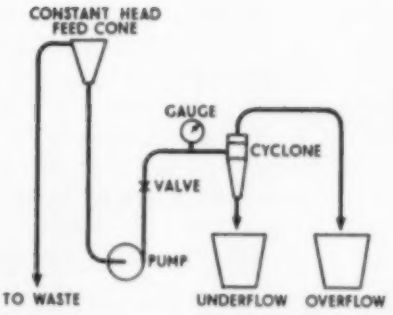

Fig. 29b. Diagrammatic arrangement of cyclone circuit for high and low pressure operations.

The main significance of this experiment is that, for a given set of cyclone conditions, some particles have a small probability of discharge due to the cyclone operation (i.e. centrifugal forces within the cyclone) through both underflow and overflow. Such particles tend to recirculate within the cyclone and are gradually eliminated by two methods. After remixing in the feed section of the cyclone a fraction joins the downward flow in which, as described in Section 3, all particles independent of size have a probability of approximately one of being discharged through the underflow. A further fraction joins the short circuit flow down the outside wall of the vortex finder and a portion is eliminated through the overflow. Some particles will be thrown out of the short circuit flow to rejoin the circulation.

This phenomenon must be of considerable importance during continuous cyclone operation since particles of a certain size range will tend to accumulate within the cyclone and result in an increase of pulp density and effective viscosity. Methods of overcoming this effect are under consideration.

5. Conclusions

For the conditions, under which the tests reported were carried out, (i.e. almost infinite dilution) the following statements can be made :

(1) For a given set of cyclone dimensions there exists a power relationship between d_{50} and feed pressure (or throughput) of the form

$$d_{50} \propto \frac{1}{P^m} \propto \frac{1}{G^n}$$

(where m and $n < 1$).

The available evidence indicates that the values of m and n are dependent on cyclone dimensions.

(2) For optimum solid elimination efficiency with a 3 in. cyclone, the feed diameter should be $\frac{1}{4}$ in. To a first approximation this feed gives optimum efficiency for all cyclone conditions, and corresponds to the conditions under which maximum rate of injection of momentum is obtained.

(3) Long, narrow rectangular feed openings give slightly improved efficiencies when compared with circular openings of the same cross-sectional areas.

(4) With large feed openings (e.g. $\frac{1}{4}$ in.) excessive turbulence in the feed section of the cyclone results in large pressure drops within the cyclone.

(5) Reduction in overflow diameter, with all other cyclone variables constant, results in increased efficiency of elimination of the finer sizes, but for coarser sizes the efficiency increases

to a maximum and decreases with further decrease in overflow diameter. This phenomenon is considered to be a direct result of the short circuit flow down the outside wall of the vortex finder.

(6) As the length of the vortex finder is decreased an increase in elimination efficiency is obtained for the finer sizes but appreciable decreases in efficiency are obtained for the coarser sizes. The latter may be attributed to the fact that practically all the coarser particles discharged through the overflow originate from the short circuit flow.

(7) Decrease in underflow diameter for the same feed pressure, with all other variables maintained constant, results in a decrease in efficiency of elimination of all particles in spite of the fact that only small decreases occur in total volume throughput.

(8) Under conditions of normal cyclone operation, particles in intermediate size ranges tend to have low probabilities of discharge through both underflow and overflow as a result of cyclone action. Such particles tend to recirculate from the lower regions of the cyclone to rejoin the mixing section near the feed opening. They leave the cyclone either by joining the short circuit flow and then leaving via the overflow, or by being carried down by the strong vertical flows near the conical cyclone wall in which all particles, independent of size, have a high probability of leaving via the underflow.

(9) From (1), (2), (5) and (6) above it is considered that no simple power relationships can be derived to describe the change in solid elimination efficiency resulting from alteration of feed opening, throughput or overflow diameter, to cover the normal operating range which must include the most efficient conditions.

Two main phenomena are responsible for the complexity of the relationships, namely, the variable degree of turbulent mixing due to "shock" effects in the feed portion of the cyclone, and the importance of the short circuit flow down the outside wall of the vortex finder.

(10) Finally, from (5) and (6) above, neither the d_{50} method for assessment of efficiency nor the method used by Fitch and Johnson can be used to describe the overall efficiency for a complete size range with any degree of significance. The only reliable method involves a comparison of efficiency curves and due consideration of the metallurgical requirements demanded of the separation.

VOL. 2 1953

Acknowledgments

Thanks are due to Mr. A. S. White, Head of Chemical Engineering Division, Atomic Energy Research Establishment, Harwell, and other members of the Division for their encouragement and advice during the investigation, to Mr. W. R. Trethewey for the excellent way in which he carried out the major portion of the experimental work, and to the Director, Atomic Energy Research Establishment for permission to publish.

References

[1] Dahlstrom, D. A.; Cyclone Operating Factors and Capacities on Coal and Refuse Slurries. Trans. A.I.M.E. (Sept. 1949) **184** 331-344.

[2] Fitch, E. B. and Johnson, E. C.; Operating Behaviour of Liquid Solid Cyclones, Min. Eng. **5** No. 3 (March 1953) 304.

[3] Kelsall, D. F.; A Study of the Motion of Solid Particles in a Hydraulic Cyclone, Trans. Inst. Chem. Engrs. **30** 1952 87.

Chemical Engineering Science, 1953, Vol. 2, pp. 273 to 281. Pergamon Press Ltd.

Fluidization and the research methods of Chemical Engineering Science*

J. CATHALA

Institut du Génie Chimique, Toulouse

(*Received* 1 *September* 1953)

Summary—Dimensional analysis in the case of fluidization, leads to expressions which apply equally well to fixed beds, to fluidized beds or to the "critical" conditions in the bed, when fluidization starts.

For porous beds, the ratio between the pressure drop and the mass velocity of the fluid expresses the resistance of the bed. This leads to the definition of the "conductivity" of the porous medium, which depends on the physical properties of the fluid, the shape of the particles and their geometrical arrangement. The latter can be represented by a function of ϵ the porosity (or voidage fraction) which is called the "vacuity" $\mathcal{V}$:

$$\mathcal{V} = \frac{\epsilon^3}{(1-\epsilon)^2}$$

For a given fluid and set of particles, the conductivity can always be represented by a function of the vacuity, $K\mathcal{V}$ for a fixed bed, and $K\mathcal{V}^n$, for a fluidized bed.

Comparison between $K\mathcal{V}$ and $K\mathcal{V}^n$ leads to an expression for v, the average velocity of translation of the solid particles in the fluidized bed.

Very few measurements are required to gather data for the control of conditions in porous beds, either fixed or fluidized.

Résumé—Appliquée à la fluidisation, l'analyse dimensionnelle permet d'établir des relations qualitatives et quantitatives qui s'appliquent aussi bien à toutes les couches poreuses, que les particules soient immobiles ou soient fluidisées et également dans cet état critique particulier ou s'amorce la fluidisation.

L'auteur montre que, pour toutes les couches poreuses, le quotient de la perte de charge par la densité de courant fluide représente la résistance de la couche à l'écoulement. Ceci conduit à définir une "conductivité" d'un milieu poreux qui dépend à la fois des propriétés du fluide, de la forme des grains et de leur répartition géométrique.

Cette dernière peut être représentée par une fonction particulière du "degré de vide" ou porosité ϵ que l'auteur propose d'appeler *vacuité* $\mathcal{V}$:

$$\mathcal{V} = \frac{\epsilon^3}{(1-\epsilon)^2}$$

Pour un fluide et un ensemble de grains donnés, la conductivité peut toujours s'exprimer par une fonction simple de la vacuité, $K\mathcal{V}$ pour une couche immobile et $K\mathcal{V}^n$ pour une couche fluidisée.

De la comparaison entre $K\mathcal{V}$ et $K\mathcal{V}^n$, on aboutit à une expression donnant v, vitesse moyenne de translation dans le lit fluidisé.

L'auteur montre comment, à l'aide de quelques déterminations expérimentales sur un échantillon de particules solides, on peut obtenir toutes les indications numériques suffisantes pour permettre d'estimer les conditions actuellement réalisées dans l'écoulement au travers de la couche poreuse, qu'elle soit immobile ou fluidisée.

Amongst the numerous unit operations which are the proper tools of the chemical engineers to meet the requirements of the chemical industry, I think that fluidization deserves special attention. In fluidized beds, we deal with an intimate mixture of solid particles and fluid flowing at such a velocity that the particles are lifted and supported by the fluid. In the particular state of fluidization,

* This was delivered as a lecture to the University of London, at University College in January, 1953.

the particles can be considered as free moving bodies : inside the bed, each of them follows an irregular course according to the chances of momentum exchanges with other particles or with the fluid. Through these repeated momentum exchanges, we achieve a very important reduction of the normal resistance to the heat and mass transfer between the solid and the fluid.

Fluidization is now one of the most useful methods of achieving exact control of all the factors regulating any chemical exchange between fluids and solids. The details of any of its many industrial applications remain outside the scope of this paper. But I consider that the development of the theory of fluidization gives a very striking example of the methods special to chemical engineering science for solving its own problems. Today, we know far more about the essentials of the theory of fluidization than we know about some very old unit operations, grinding for instance.

Like any scientist, before any attempt towards theory, the chemical engineer must start some experiments. He will determine for instance the relation between the flow of some particular fluid and the pressure drop through a bed of solid particles. He can measure u the linear velocity of the fluid or preferably the mass velocity, G, mass of fluid crossing in a unit of time the unit of section of the empty column. Usually called " mass velocity," G is a current density and its relation to the linear velocity is given by :

$$G = u\,\rho \qquad G \equiv M\,\theta^{-1}\,L^{-2}$$

The laws governing the flow of fluids through porous beds are well known and between very large limits the pressure drop ΔP remains proportional to the mass velocity (Fig. 1). When G becomes very high, the pressure drop increases more slowly than the mass velocity. Finally, the mass velocity can continue to increase at a practically constant pressure drop : we have a fluidized bed. But if we stop the flow and start again our experiments, we observe new values for G or ΔP : they vary according to the conditions of our bed.

To give a quantitative representation of these conditions of our porous bed, we will call " packing fraction " τ (in French, " tassement ") the ratio

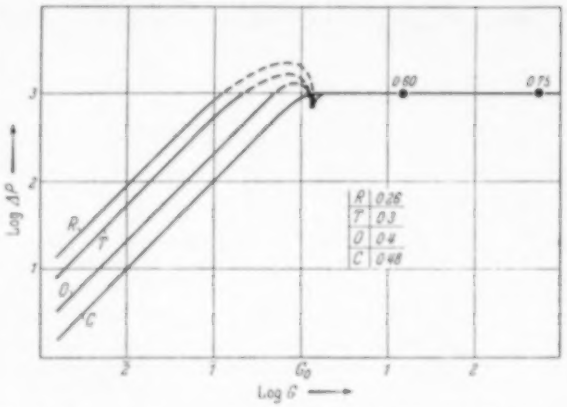

Fig. 1. Pressure drop and rate of flow (spheres of uniform diameter).

of the occupied volume to the apparent volume. We will call " voidage fraction " or porosity ϵ the ratio of the voids to the apparent volume. We are also interested in the specific height of our bed which can be expressed as the height of a unit of mass of particles in a column of unit area. The specific height A is obviously related to the apparent volume and we have : $\tau A = 1/\rho'$; $\epsilon + \tau = 1$.

Dealing for instance with regular spheres of constant diameter, we know that the porosity will vary according to pure geometrical laws, from a minimum value 0·259 for a rhombohedral distribution to a maximum 0·476 for a cubic distribution. It is convenient to take as a unit the specific height of our bed at its maximum porosity ϵ_0.

To obtain reproducible determinations in our fluidization experiments, we must start with a bed of maximum porosity, ϵ_0. For beds with closer packing, before fluidization starts, we have some local rearrangements of our spheres, and a corresponding increase of the free area for the flow with a small decrease in the pressure drop. With proper care, we observe a well-pronounced break in our curves : fluidization *starts just above a threshold* and requires a *critical value* G_0 for the mass velocity.

Before this threshold, when G grows, the pressure drop increases, as the increased velocity increases the friction against the walls of the small irregular channels of our bed. Inversely,

VOL. 2 1953

through the friction, every sphere suffers an increased vertical pressure, opposed to its weight. For a certain critical velocity, G_0, the friction forces exactly balance the gravity : our spheres remain still tangent together, but they cease to support each other. For a very small increase above G_0, the spheres are separated and we are in the fluidized condition.

We know that the friction forces will be a certain function of the diameter of our spheres, will be proportional to the linear velocity, and will depend on the viscosity of our fluid. These friction forces will be equal to the weight of our particles, which is proportional to some function of their diameter, their buoyancy and g. We can write :

$$\alpha\, d^x\, (\rho' - \rho)^n\, g^n = u_0\, d^y\, \mu^z$$

$$G_0 = u_0\, \rho \qquad G_0 = \alpha\, d^m\, (\rho' - \rho)^n\, \rho\, g^n / \mu^z$$

From the dimensional analysis of the critical conditions before fluidization starts, we can obtain the values for the exponents m, n and z :

$$m = 2 \qquad n = z = 1$$

G_0 will be proportional to the buoyancy of our particles, to the specific gravity of our fluid, to the reciprocal of its viscosity and to the *square of the diameter* of our spheres. The height of our bed does not appear in our formula. In fact, at the critical point, the same critical velocity will totally support beds of very different heights. But the pressure drop will increase proportionally to the height.

Now we will gather the answer from the experiments. Without going into the details of the many determinations published for critical mass velocity, we will give briefly some significant results. LEVA [1] and colleagues' results can be summarized by the relation :

$$G_0 = 0{\cdot}005\, \frac{\epsilon_0^{\,3}}{(1 - \epsilon_0)} \cdot \frac{d^2}{\phi^2}\, (\rho' - \rho)\, \rho\, g / \mu$$

MILLER and LOGWINUK [2] propose the following expression :

$$G_0 = 0{\cdot}00125\, d^2\, (\rho' - \rho)^{0{\cdot}9}\, \rho^{1{\cdot}1}\, g / \mu$$

Assuming perfect spheres of constant radius in MILLER's experiments, with $\epsilon_0 = 0{\cdot}476$; $\epsilon_0^3/1 - \epsilon = 0{\cdot}2065$, their relation becomes :

$$G_0 = 0{\cdot}00605\, \frac{\epsilon_0^{\,3}}{1 - \epsilon_0} \cdot d^2\, (\rho' - \rho)^{0{\cdot}9}\, \rho^{1{\cdot}1}\, g / \mu$$

For VAN HEERDEN [3] and colleagues the critical mass velocity is given by :

$$G_0 = 0{\cdot}0065\, \frac{\epsilon_0^{\,3}}{1 - \epsilon_0} \cdot \frac{d^2}{\beta}\, \rho' \cdot \rho \cdot g / \mu$$

The concordance between the three sets of experiments is impressive and we come to the conclusion that our dimensional analysis of the conditions existing at the starting point of fluidization is correct. G_0 varies with the square of d, with the expected dependence on the specific gravities and viscosity. But we have not yet obtained any information on the pressure drop, necessary to maintain the mass velocity G_0.

To go further, we will remember that, in the critical stage we consider that our particles are still in material contact together. Except for the amount of pressure between the particles, at the critical point, no differences exist in the conditions of the porous bed and it is legitimate to apply the well known laws on the flow of fluids through porous bed. Since the researches of KOZENY [4] and CARMAN [5], we know that POISEUILLE's law applies with some modifications imposed by the irregular shape of our small channels :

$$\frac{dP}{dL} = 32\, u_c\, \mu\, \frac{1}{d_c^2}$$

$$u_c\, \epsilon = u$$

$$a = N \cdot \pi\, d_c / \tau\, \pi\, \frac{D^2}{4}$$

$$N\, \pi\, d_c^2 / 4 = \pi\, D^2\, \epsilon / 4$$

$$d_c = \frac{4\, \epsilon}{1 - \epsilon} \cdot \frac{1}{a}$$

$$\frac{dP}{dL} = 2\alpha\, \frac{(1 - \epsilon)^2}{\epsilon^3} \cdot \mu\, u\, a^2$$

$$\alpha = \left(\frac{\pi}{2}\right)^2 = 2{\cdot}467 = 2{\cdot}5$$

$$a = \pi\, d^2 / \frac{1}{6}\, \pi\, d^3 = 6/d \ldots 6\, \phi/d$$

$$(a) \qquad \frac{\Delta P}{L} = 180\,\frac{(1-\epsilon)^2}{\epsilon^3}\cdot\mu\,\frac{G}{\rho}\cdot\frac{\phi^2}{d^2}$$

$$(b) \qquad (\rho' - \rho)\,g\,(1-\epsilon_0) = \frac{\Delta P}{L} = 180\,\frac{(1-\epsilon_0)^2}{\epsilon_0^3}\cdot\mu\,\frac{G_0}{\rho}\cdot\frac{\phi^2}{d^2}$$

$$(c) \qquad G_0 = 0{\cdot}0055\,\frac{\epsilon^3{}_0}{1-\epsilon_0}\cdot\frac{d^2}{\phi^2}\cdot(\rho' - \rho)\,\rho\,g/\mu$$

Not only did we find the same form of dependence between G_0 and the porosity supported by the experiments of LEVA and VAN HEERDEN, but the numerical value of the constant lies between the extreme values found in the experimental work.

To obtain in expression (*c*) the value of G_0, the critical mass velocity when fluidization starts, we make in (*b*) the pressure gradient $\Delta P/L$ as given in (*a*) equal to the weight of all the particles present in a volume unity : our theory is based on the assumption that all these particles are supported now by fluid friction.

But expression (*a*) applies to all fixed beds of porous particles and shows the interdependence between mass velocity G, pressure gradient $\Delta P/L$ and the variable porosity ϵ of any bed of definite particles. The four different straight lines in Fig. 1 correspond to the values taken by ϵ when spheres of constant diameter are assembled together in regular geometrical arrangement :

$\epsilon_R = 0{\cdot}259$ rhombohedral packing.
$\epsilon_T = 0{\cdot}302$ tetragonal packing.
$\epsilon_0 = 0{\cdot}395$ orthorhombic packing.
$\epsilon_C = 0{\cdot}476$ cubic packing.

To each value of the porosity corresponds a value of the specific height of the bed of particles (Fig. 2).

$$\text{Packing fraction } \tau = \frac{v'}{v} = \frac{M}{\rho' v}$$

$$\text{Porosity } \epsilon = \frac{v - v'}{v} = 1 - \tau$$

$$\text{Specific height} \qquad \Lambda = 1/\rho'\,\tau.$$

It is worthwhile to transform expression (*a*) :

$$\frac{G\,L}{\Delta P} = 0{\cdot}0055\,\frac{\rho}{\mu}\cdot\frac{d^2}{\phi^2}\cdot\frac{\epsilon^3}{(1-\epsilon)^2}$$

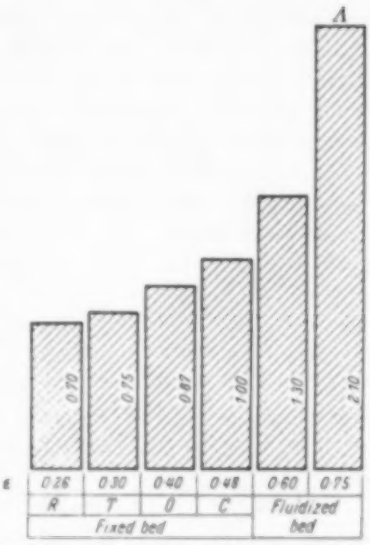

Fig. 2. Specific height of porous beds (spheres of uniform diameter).

Here as well as in all its transfer problems, chemical engineering science finds a generalized form of OHM's law :

$$\frac{\text{Driving force}}{\text{Rate of flow}} = \text{Resistance}$$

$$E = IR = I\cdot\rho\,\frac{L}{S} \qquad \frac{I}{S}\cdot\frac{L}{E} = \frac{1}{\rho} = \kappa$$

The quotient of the current density by the gradient of the driving force is the *reciprocal of a resistivity* : it is a *conductivity*. The conductivity corresponding to this transfer problem has the dimension of time.

In relation (*c*), we will note that, at the critical point, the current density is identical with the product of the bed's conductivity by the apparent weight of all the particles enclosed in a volume unity :

$$G_0 = 0{\cdot}0055\cdot\rho/\mu\cdot d^2/\phi^2\cdot\frac{\epsilon_0^3}{(1-\epsilon_0)^3}\cdot(\rho' - \rho)\,g\,(1-\epsilon_0)$$

In the mathematical expression of the conductivity of a porous bed, it is obvious that we shall find a term related to the physical properties of the moving fluid : this property is the reciprocal of its kinematic viscosity. Leaving apart the " kinematic fluidity " of the fluid, our expression

VOL. 2 1953

of the conductivity gives the " permeability " of the bed, a characteristic property depending upon the diameter and shape of the particles (terms d^2/ϕ^2) and upon their geometrical distributions. We propose to call " vacuity " of the bed and to represent by the symbol $\mho$ the term $\epsilon^3/(1-\epsilon)^2$ which describes the arrangement, and we can write for any porous bed :

conductivity = (kinematic fluidity) (area of equiv. sphere) (vacuity).

$$\frac{G\,L}{\Delta\,P} = (\rho/\mu)\,(d^2/\phi^2)\,0{\cdot}0033\left(\frac{\epsilon^3}{(1-\epsilon)^2}\right)$$

For a given fluid, it is clear that the conductivity of all porous beds made with the same particles, is a linear function of the vacuity of the bed :

$$\frac{G\,L}{\Delta\,P} = K\,\mho$$

From direct measurement of the height L of a porous bed of constant area S, and containing a mass M of particles in a volume V, we can obtain the specific conductivity of the porous bed of unit area and specific height Λ, corresponding to a mass unity. The pressure drop takes a new numerical value but the general expression still remains :

$$\frac{G\,\Lambda}{\Delta\,P} = K\,\mho$$

When the porosity varies between 0 and 1, the vacuity can take any value between 0 and infinity. Table 1 gives the corresponding values of ϵ, $\mho$, and $\log \mho$.

In any porous bed of constant area S, it is always possible to measure L and G in various conditions of the porous bed : fixed bed or fluidized bed. From L, it is easy to obtain Λ, then $\epsilon = 1 - 1/\rho'\,\Lambda$ and finally the present value of $\mho$. Table 1 gives a series of values for $K\,\Lambda$ and $\log K\,\Lambda$, K being $\rho'\,(1-\epsilon_0)$ and ϵ_0 taken equal to 0·476, its normal value for a bed of spheres of constant diameter.

Dealing with fluidized beds, when ΔP remains constant and equal to ΔP_0 (the value at the critical point), LEVA has been able to show that the conductivity grows with the nth power of the vacuity. The experimental values of n vary between 2·5 and 3·5, according to the size and shape of particles ; n remains independent of the nature of the fluid.

$$\frac{G_f\,\Lambda}{\Delta\,P_0} = K\,\mho^n$$

Now we can imagine an " expanded " bed as opposed to a fluidized bed. In the " idealized " conditions of our expanded bed, the specific height will be the same, the average value of the mean distance between our particles will remain the same as in the fluidized state but our particles will remain immobile : exactly like in a porous bed, the conditions of an expanded bed can be represented by a straight line of slope unity.

For every value of the vacuity, we have a definite value for G_f and for G_e, the mass velocities corresponding to this fluidized and " idealized " conditions. LEVA calls fluidization efficiency the value of the ratio.

$$\frac{G_f - G_e}{G_e} = \eta$$

This ratio is very useful to appreciate the intensity of the agitation in fluidized beds.

We will remember that Pressure multiplied by Volume gives Work. The product of the pressure drop by the total rate of flow through the entire bed gives the power required to maintain the bed in the fluidized or in the " expanded " state.

Fluidized conditions :

$$W_f = \Delta P \,.\, \pi\, D^2/4 \,.\, G_f/\rho$$

Expanded state :

$$W_e = \Delta P \;.\; \pi\, D^2/4 \;.\; G_e/\rho$$

From the difference, we obtain the power required to maintain the agitation of our particles in the fluidized bed.

$$W_a = W_f - W_e = \Delta P \;.\; \pi\, D^2/4 \;.\; G_f \;.\; \eta/\rho$$

Such a power is consumed by friction, each individual particle moving with an average velocity v hitting many times the other bodies. Calling F a friction factor we have :

$$W_a = F\,g\,v\,\Sigma\,m$$

where, for the critical conditions, we have :

$$\Sigma m = \rho' \tau_0 A_0 \pi D^2/4 \qquad \frac{\Delta P_c}{A_0} = (\rho' - \rho) \tau_0 g$$

and remembering that for fluidized bed $\Delta P = constant = \Delta P_c$, we obtain the value of the mean velocity of our particles in a fluidized bed.

$$v = G_f \cdot \eta / F \cdot \left(\frac{1}{\rho} - \frac{1}{\rho'}\right)$$

In this way, we have developed some kind of kinetic theory of our fluidized state and we are now in a position to attempt some analysis of the conditions of heat transfer in a fluidized bed.

It is classical in heat transfer problems to refer to h, the heat transfer coefficient, the dimensions of which are $M \theta^{-3} T^{-1}$: h depends from both the properties of the system and the conditions of flow.

The properties of the system governing the heat transfer will probably be its thermal conductivity k, its viscosity μ, its specific mass ρ and its heat capacity C, and the conditions of flow which shall be represented by the value of v, the average velocity of our particles, and by some linear dimensions D. We can now write a general expression of h :

$$h = \alpha \mu^x \rho^y v^z k^p C^q D^r$$

and the dimensional analysis leads immediately to an expression of classical form :

$$\frac{h D}{k} = \alpha \left(\frac{C \mu}{k}\right)^q \cdot \left(\frac{D v \rho}{\mu}\right)^{r+1} = \frac{\alpha}{F^{r+1}} \cdot \left(\frac{C \mu}{k}\right)^q \cdot \left(\frac{D G_f \eta}{\mu}\right)^{r+1}$$

The experimental determinations of h for fluidized beds are not very numerous ; their results are often contradictory. From his experiments, LEVA considers that q and r can be neglected and gives for the heat transfer coefficient :

$$h = \frac{\alpha}{F} \cdot k \, G_f \eta / \mu$$

We think that the experiments of LEVA are not sufficient to prove that linear dimensions are without influence on the heat transfer coefficient. The fluidization efficiency depends for a particular bed on the value of the slope of the fluidization line and this slope varies with the diameter of the particles. Some authors have found explicit influence of this diameter but from our dimensional analysis, we know now that to detect the role of linear dimensions, it cannot be sufficient to experiment with particles of different diameter or shape in the same column, but it is essential to vary also the size of the bed.

It is very convenient to represent on a graph (Fig. 3), the relationships between all the characteristics properties of the flow through our beds.

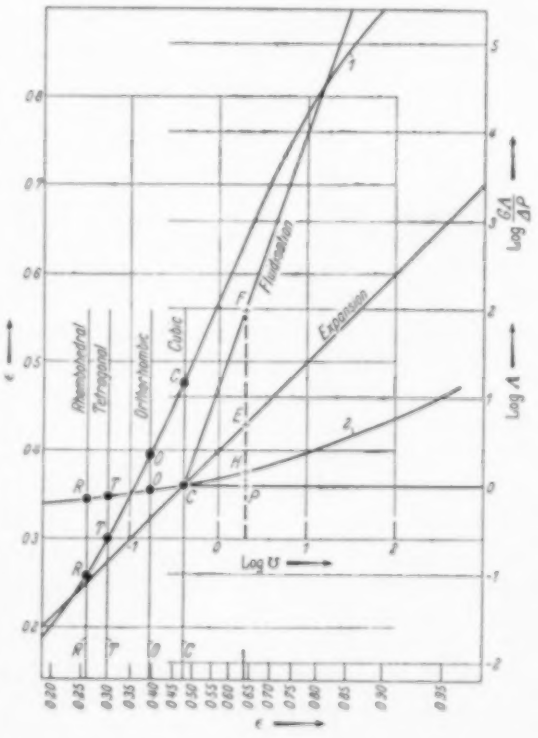

Fig. 3.

Curve 1 represents the relation between ϵ (ordinate axis) and log $\mathfrak{V}$ (abscissa axis). From curve 1, it is useful to transfer the values of the porosity on a horizontal line. Curve 2 gives the values of log Λ as a function of log $\mathfrak{V}$.

We have given in Table 1, the series of numerical data needed for the construction of curves 1 and 2. According to our theory, curves 1 and 2, with

VOL. 2 1953

Table 1.

ϵ	$K\Lambda$	log $K\Lambda$	σ	log σ	*Observations (spheres of uniform diam.)*
0·1	0·585	− 0·233	0·00123	− 2·910	
0·2	0·655	− 0·184	0·0125	− 1·903	
0·25			0·028	− 1·156	
0·26	0·70	− 0·155	0·032	− 1·495	Rhombohedral, minimum porosity
0·3	0·748	− 0·126	0·055	− 1·260	
0·302	0·75	− 0·125	0·056	− 1·252	Tetragonal
0·35			0·101	− 0·996	
0·395	0·87	− 0·06	0·166	− 0·78	Orthorhombic
0·476	1	0	0·393	− 0·406	Cubic, maximum porosity
0·500	1·05	0·021	0·5	− 0·301	
0·55			0·821	− 0·086	
0·565	1·20	0·079	1	0	
0·6	1·3	0·114	1·35	0·130	
0·65			2·24	0·35	
0·666	1·57	0·196	2·66	0·425	
0·7	1·75	0·243	3·81	0·581	
0·75	2·1	0·322	6·75	0·829	
0·80	2·6	0·415	12·8	1·107	
0·85	3·49	0·543	27·3	1·436	
0·9	5·25	0·720	72·9	1·863	
0·95	10·5	1·02	343	2·535	

their corresponding scales apply to any kind of fluid flow through any kind of porous bed.

The control of any fluidized process requires the knowledge of the conductivity of our bed and the average velocity of our particles. Few experimental determinations are needed but they can be achieved on a small scale, at normal temperature, and with air for which accurate kinetic fluidity values are readily available.

For any kind of particle, of variable size and shape, it is always possible to measure the porosity of the bed when we know the specific mass ρ'. In a column of constant section S, we will dispose a mass M of particles and measure the height of the bed L : we obtain immediately $\Lambda = LS/M$ and the packing fraction or the porosity : $\tau = 1 - \epsilon = \rho' \Lambda$.

It is worthwhile to measure various values of the porosity for various conditions of packing. Dealing with air, we can measure, for every conditions of packing, the values of the mass velocity G and pressure drop ΔP. In this way, we can obtain a reliable experimental value of d^2/ϕ^2. For irregular particles, it seems that the correct value of the dimaeter of the equivalent sphere is more accurately obtained when operating the bed at its minimum porosity.

To obtain the maximum porosity, we will increase the rate of flow until fluidization conditions are well established. By reducing gently the rate of flow, we can measure Λ_0 and ϵ_0. As explained before, it is convenient to take Λ_0 as the unity of specific height for our beds. Accordingly, in Fig. 2, the point corresponding on curve 2 to log σ_c (and to ϵ_0 on the horizontal scale) will be taken as the origin of the vertical scale of log Λ.

When we carry out the determinations of Λ_0 and ϵ_0, we can measure also together G_0 and ΔP_0. It is also convenient to take the same point as the origin of the vertical scale for the function $\log \dfrac{G\,\Lambda}{\Delta P}$. This is equivalent to take for respective units G_0 the critical mass velocity, and ΔP_0 the pressure drop, together with Λ_0. Dealing with mass velocities above G_c, can measure different values of $G_f = 2\,G_0 \ldots 4\,G_0 \ldots 6\,G_0$ and obtain the corresponding values of L, Λ, ϵ,

$\mathcal{V}$. In fluidized conditions the pressure drop remains constant ΔP_0. It is easy to obtain the value of the exponent n in the expression :

$$\frac{G_f L}{\Delta P_0} = K \mathcal{V}^n$$

equivalent to :

$$\log G_f A = n \log \mathcal{V} + constant$$

In Fig. 3, this corresponds to a straight line, of slope n, which we start from our chosen origin. A straight line of slope 1, corresponds below curve 2 to the flow conditions in fixed beds and above curve 2, to the "idealized" expanded bed. In Fig. 3, we have taken for ϵ_0 the value 0·476, maximum porosity of a bed of spherical particles with constant diameter.

Once constructed for a definite set of particles, for the control of any fluidized bed, the graphs of Fig. 3 give immediately all the necessary data by the single determination of the pressure drop through a known height of the bed. From this, we can deduce the present value of the specific height. In our graph, curve 2 gives $\log A =$ segment $P H$; we obtain directly the logarithm of the present mass velocity G_f (segment $H F$) ; the present value of $\log G_e$ is given by segment $H F$. We obtain easily the fluidization efficiency and the average velocity of our particles.

If instead of working our bed with air at normal temperature, we deal with any other gas in different conditions of temperature and pressure we can utilise our graph by converting the critical mass velocity with air at normal temperature to the new value of the critical velocity by introducing the ratio of the values of the kinematic fluidity in the two sets of conditions (we can neglect the effect on the buoyancy of the particles of the change in specific gravity of the gases).

I do not pretend that the above theory is either complete or definitive : many important details have been left out. In our kinetic theory of the fluidized bed, we have been compelled to accept coarse simplifications. In practice, our particles are neither spherical nor uniform in size. Many experiments and plenty of work remain to be done before achieving a complete analysis of the mechanism of fluidization : we need for instance better methods of expressing the size distribution of our particles ; until now, the influence of their shape has been completely neglected. Nevertheless, we are now able to give with some accuracy the basic data for the design of a fluidized bed converter.

When we remember that the large utilisation of fluidization is not yet ten years old, it is clear that theory has not been slow in superceding empiricism. I think that we can recognize a true science when we find any organized knowledge helping us to solve some problems by its own methods. Fluidization is for me a sound example of the special methods which belong to chemical engineering science.

VOL. 2 1953

NOMENCLATURE

Symbol	*Dimension*	*Signification*
a	L^{-1}	Specific area of a particle
C	$L^2 \theta^{-2} T^{-1}$	Heat capacity of the fluid
d	L	Diameter of the equivalent sphere to a particle
d_e	L	Diameter of channel for flow in porous bed
D	L	Diameter of the fixed or fluidized bed
F	0	Friction factor
g	$L \theta^{-2}$	Acceleration of gravity
G	$M L^{-2} \theta^{-1}$	Mass velocity of the fluid (empty column)
h	$M \theta^{-3} T^{-1}$	Heat transfer coefficient
k	$M L \theta^{-3} T^{-1}$	Thermal conductivity
L	L	Present height of the bed
N	O	Number of channels in the section of the bed
ΔP	$M L^{-1} \theta^{-2}$	Pressure drop through the bed
u	$L \theta^{-1}$	Linear velocity (empty column)
v	$L \theta^{-1}$	Average linear velocity of a particle in fluidized bed
W	$M L^2 \theta^{-3}$	Power required for maintaining flow conditions

Symbol	*Dimension*	*Signification*
m, n, p, q	0	As exponents
x, y, z	0	As exponents
$,$	0	As exponent for specific proportion of the particle
0	0	As subscript, characteritic of critical conditions
f	0	As subscript, characteristic of fluidization
e	0	As subscript, characteristic of expansion
a	0	As subscript, characteristic of agitation of bed
A	$M^{-1}L^3$	Specific height of the bed in present conditions
μ	$M\,L^{-1}\,\theta^{-1}$	Fluid viscosity
ρ	$M\,L^{-3}$	Specific gravity
α	0	Numerical factor
ϵ	0	Porosity of the bed
η	0	Fluidization efficiency
τ	0	Packing fraction of the bed
ϕ	0	Shape factor of the particle
Ω	0	" Vacuity " of the bed ($\Omega = \epsilon^3/(1-\epsilon)^2$)

REFERENCES

[1] LEVA, M., GRUMMER, M., WEINTRAUB, M. and POLLCHICK, M. ; Chem. Eng. Prog. 1948 **44** 551, 619.
Ind. Eng. Chem. 1949 **41** 1206.

LEVA, M., WEINTRAUB, M. and GRUMMER, M. ; Chem. Eng. Prog. 1949 **45** 563.

[2] MILLER, C. and LOGWINUK, A. K. ; Ind. Eng. Chem. 1951 **43** 1220.

[3] VAN HERDEN, C., NOBEL, A. P. P. and VAN KREVELEN, D. W. ; Chem. Eng. Sc. 1951 **1** 37.

[4] KOZENY, J. ; Sitzber Akad, Wiss. Wien 1927 **136a** 271.

[5] CARMAN, P. C. ; Trans. Inst. Chem. Eng. (Lond.)—1937 **15** 150.
Trans. Inst. Chem. Eng. (Lond.)—1937 **16** 168.
J. Soc. Chem. Ind. – 1933 **52** 280.
J. Soc. Chem. Ind. – 1934 **53** 139.
J. Soc. Chem. Ind. – 1938 **57** 225.
J. Soc. Chem. Ind. – 1939 **58** 1.

Chemical Engineering Science, 1953, Vol. 282, pp. 2 to 286. Pergamon Press Ltd.

Extraction of Acetic acid from water

2. Ethyl acetate—acetic acid water

F. H. Garner and S. R. M. Ellis

The Chemical Engineering Dept., The University, Birmingham, 15

(*Received* 11 *November* 1953)

Summary—Solubility and liquid-liquid equilibrium data are given for the system ethyl acetate-acetic acid-water at 30°C, 40°C, and 50°C ; the solubility curve and distribution ratio are affected only slightly by change in temperature. The predicted distribution coefficients are lower than experimental coefficients. Papers are to follow giving the vapour-liquid equilibrium data for the system ethyl acetate-water-acetic acid.

Résumé—Présentation pour le système acétate d'éthyle – acide acétique – eau à 30°C – 40°C – 50°C, des solubilités et des compositions d'équilibre liquide-liquide ; les variations de température agissent très peu sur les couches de solubilité et sur les coefficients de distribution. Les valeurs calculées pour ces dérniérs sont plus faibles que les valeurs expérimentales.

Pour le même système, d'autres mémoires suivront pour donner les valeurs relatives à l'équilibre liquide – vapeur.

Introduction

Eaglesfield, Kelly and Short [14] have suggested that for less than 15·0 per cent by weight of acetic acid in the feed, ethyl acetate is one of the best solvents available. Above 15·0 per cent by weight of acetic acid in the feed, the ethyl acetate may be mixed with a proportion of benzene.

Although the system ethyl acetate-acetic acid-water is important, industrially the published data is of a limited nature. The mutual solubility curve was determined by Mion [15] at 30°C. Tie line or liquid-liquid equilibrium results were reported by Sohoni and Warhadpande [16] for 30°C while Eaglesfield, Kelly and Short [14] give distribution coefficient data for 15·0°C. Roy [17] using the apparatus described by Hunter and Nash [5] determined equilibrium data at 30°C and 40°C. Equilibrium results were also obtained by Roy [17] at 50°C and 60°C by using a stoppered flask.

It was thought desirable that the results of Roy [17] should be repeated using a modified form of the equilibrium apparatus of Smith and Bonner [18].

Purity of Materials Used

Analytical grade chemicals and a laboratory source of distilled water were used. Ethyl acetate and benzene were fractionated in a thirty plate column at a reflux ratio of 25:1. The solvents and the acid were tested for purity by refractive index and boiling point determinations.

Substance	*Refractive Index at 20°C*	*Boiling Point °C*
Water	1·3320	100·0
Acetic acid	1·3680	118·5
Ethyl acetate	1·3700	77·1
Benzene	1·5011	80·1

Experimental

The method of analysis of acetic acid and the determination of solubility data was as discussed in Part 1 benzene-acetic acid-water [19].

The tie line data was determined in a modified form of the apparatus of Smith and Bonner [18].

Solubility data for ethyl acetate-acetic acid-water at 30°, 40°, 50° and 60°C is given on Table 4. Table 5 gives further solubility results at 30°C for the system 85/15, ethyl acetate/benzene-acetic acid-water.

Equilibrium or tie line data for the system ethyl acetate-acetic acid-water at 30°, 40° and 50°C is given in Table 6.

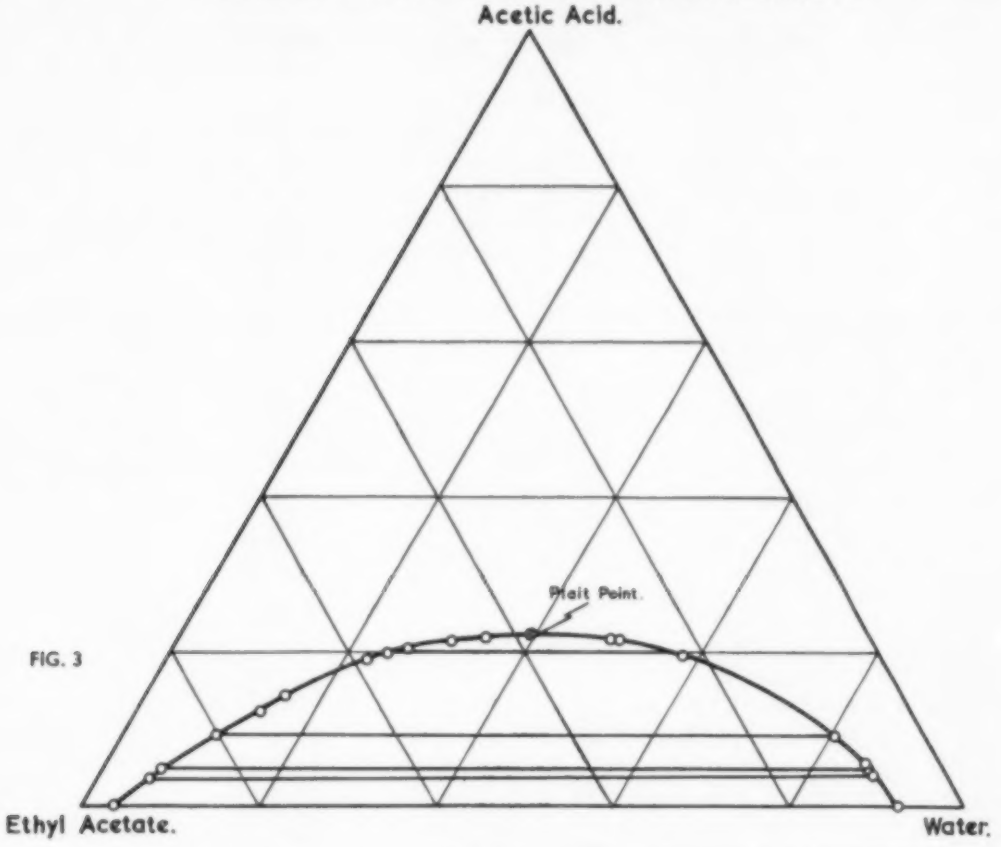

FIG. 3

DISCUSSION OF RESULTS

A comparison of the results given on Table 4 shows that the spread of the solubility curve decreases only slightly with temperature. The equilibrium data is almost independent of temperature changes.

Fig. 3 shows the equilibrium data at 30°C plotted on triangular graph paper. These results and those at 40°C and 50°C are satisfactorily correlated by BACHMAN [6] and OTHMER-TOBIAS [7] plots. Fig. 4 plots the equilibrium data as a distribution curve and compares the results of several investigators. The experimental results given here are in close agreement with those of SOHONI and WARHADPANDE [16] and of HAUGHTON [20] determined at 25°C. The data of EAGLESFIELD, KELLY and SHORT [14]

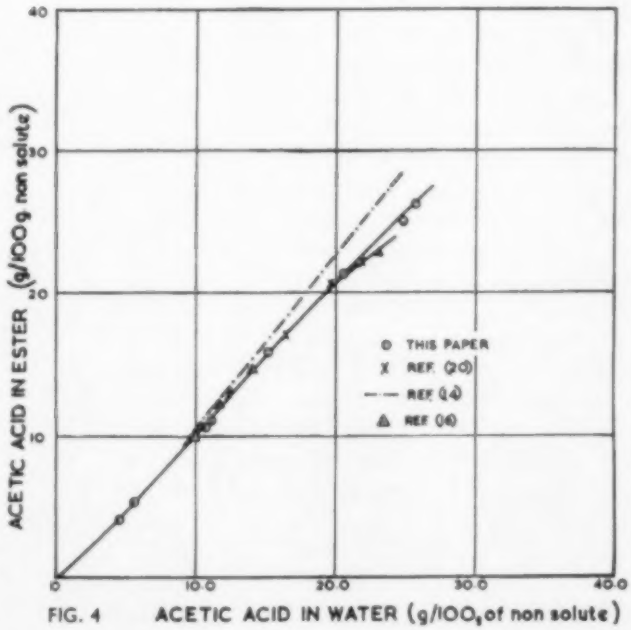

FIG. 4

Table 4

Ethyl Acetate-Acetic Acid-Water. Solubility Data

t°C	*Acetic Acid gm*	*Water gm*	*Ethyl Acetate gm*
30	4·9	6·4	88·7
	4·9	6·1	89·0
	12·4	14·0	73·6
	14·8	15·5	69·7
	20·8	26·2	53·0
	22·0	34·4	43·6
	21·8	48·9	29·3
	5·8	85·9	8·3
	9·3	80·3	10·4
	21·8	49·6	28·6
	21·7	31·1	47·2
	19·3	22·4	58·3
40	4·9	6·5	87·6
	9·4	10·6	80·0
	13·2	14·0	72·8
	17·8	21·0	62·2
	20·2	28·3	52·5
	21·2	37·0	41·8
	4·3	88·0	7·7
	10·0	80·0	10·0
	13·5	74·2	12·3
	17·0	16·5	66·5
	20·2	54·0	25·8
50	4·9	7·5	87·6
	9·4	10·7	79·9
	13·2	14·0	72·8
	14·4	16·5	69·1
	17·7	21·6	60·6
	19·6	27·8	52·6
	20·6	37·2	42·2
	5·8	86·3	7·9
	9·3	80·9	9·8
	14·1	72·6	13·3
	17·0	65·0	18·0
	19·3	55·0	25·7
60	5·0	6·7	88·3
	15·0	15·0	70·0
	18·5	26·0	55·5
	18·7	28·0	53·3
	4·8	86·7	8·5
	7·2	83·7	9·1
	13·0	73·9	13·1
	16·3	66·3	17·4
	19·0	56·5	24·5

give a higher distribution coefficient in favour of ethyl acetate at high concentrations of acetic acid.

For the system 85/15 ethyl acetate/benzene-acetic acid-water only a few equilibrium determinations have been made. With a 19·5 per cent concentration of acetic acid in the solvent layer there is a concentration of 24·0 per cent acetic acid in the aqueous layer.

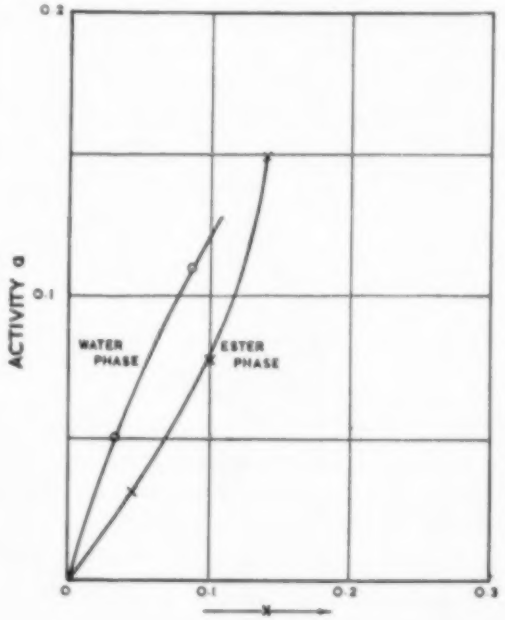

FIG. 5

Table 5

85/15 *Ethyl Acetate/Benzene-Acetic Acid-Water. Solubility Data*

t°C	*Acetic Acid gm*	*Water gm*	*Ethyl Acetate gm*
30	9·6	6·6	83·8
	20·3	15·1	64·6
	29·6	30·6	39·8
	30·6	33·5	35·9
	32·7	38·3	29·0
	36·5	48·5	15·0
	36·0	50·0	14·0
	29·0	65·7	5·3
	20·7	76·5	2·8
	20·0	77·2	2·8
	0·0	98·3	1·7

VOL. 2 1953

Table 6

Ethyl Acetate-Acetic Acid-Water. Tie Line Data

t°C	Ester Phase			Water Phase			Plait Point		
	% Acid	% Ester	% Water	% Acid	% Ester	% Water	% Acid	% Ester	% Water
30	3·9	90·1	6·0	4·3	8·0	87·7			
	20·0	55·0	25·0	19·8	23·0	57·2			
	9·6	80·4	10·0	9·6	10·0	80·4	22·5	38·3	39·2
	4·9	89·1	6·0	5·2	8·0	86·8			
40	4·9	89·1	6·0	5·2	8·0	86·8			
	9·8	80·3	9·9	10·0	10·0	80·0			
	20·6	54·6	24·8	19·8	23·1	51·1	21·5	38·8	39·7
	3·90	90·1	6·0	4·3	8·0	87·7			
50	5·0	89·0	6·0	5·6	8·0	86·4			
	10·1	80·4	9·5	10·0	10·0	80·0			
	20·8	54·5	24·7	20·2	23·0	56·8	21·0	39·0	40·0
	10·0	10·0	80·0	9·8	10·0	80·2			

In the above table all percentages are by weight

PREDICTION OF EQUILIBRIUM DATA

The vapour liquid equilbria data of BROWN and EWALD [21] for acetic acid-water and that of PEARCE [22] for ethyl acetate-acetic acid, have been used to calculate ternary activity coefficients for acetic acid over a range of compositions on the solubility curve. The above binary activity coefficient plots were approximately corrected for temperature effects by assuming that $T \log \gamma$ is constant. Since those binary systems are not satisfactorily correlated by the Margules and van Laar equations, linear interpolation has been used to calculate the ternary activity coefficients. The resulting activity composition plots are shown on Fig. 5.

A comparison between predicted and experimental distribution ratios is given on Table 7.

There is resonable agreement between the experimental and predicted results except for 9·6 per cent by weight of acetic acid in the water phase.

The above comparison between experimental and predicted results must, however, be treated with caution since the order of the activity coefficients for acetic acid in the two binary systems is quite low and thus susceptible to error. Furthermore there are association effects and some doubts as to the validity of using linear interpolation for predicting ternary activity coefficients.

Table 7

Acetic acid in water phase		Distribution Ratio = $\frac{\text{Mole \% acid in ester phase}}{\text{Mole \% acid in water phase}}$	
Weight %	Mole %	Experimental	Predicted
19·8	8·7	1·6	1·45
9·6	3·4	2·9	2·1
4·3	1·9	2·4	2·4

Solutropy

As the selectivity of acetic acid for ethyl acetate reverses at a certain stage and then becomes selective towards water, Sohoni and Warhadpande [16] state this system is a solutrope at 9·5 per cent by weight of acetic acid in the water layer. From Table 7 it can be seen that on a molal basis the distribution coefficient is always greater than unity, and thus no molal solutrope exists.

At 9·6 per cent by weight of acetic acid in the water layer the mole per cent distribution ratio reaches a maximum value. Furthermore, at this point there is the greatest deviation between predicted and experimental distribution ratios. This discrepancy in the distribution ratios at the weight solutrope composition may imply there is a change on the degree of association in one of the phases.

In the evaluation of the ternary activity coefficients the same molecular weight has been used for acetic acid in the two binary systems.

References

[14] Eaglesfield, P., Kelly, B. K., and Short, J. F.; Industrial Chemist, 1953 **29** 147, 243.
[15] Mion; Compt. Rend. 1931 **193** 1330.
[16] Sohoni, V. R. and Warhadpande, U. R.; Ind. Eng. Chem. 1952 **44** 1428.
[17] Roy, U. N. G.; M.Sc. Thesis, Chem. Eng. Dept., The University, Birmingham, 1948.
[18] Smith, T. E. and Bonner, R. F.; Ind. Eng. Chem. 1950 **42** 896.
[19] Garner, F. H., Ellis, S. R. M. and Roy, U. N. G.; Chem. Eng. Sci. 1953 **2** 14.
[20] Haughton, C. O.; Private Communication, Courtaulds Ltd.
[21] Brown, I. and Ewald, A. H.; Australian J. Scientific Res. 1950 **3** 306.
[22] Pearce, C. J.; Ph.D. Thesis, Chemical Engineering Dept., The University, Birmingham, 1953.

VOL. 2 1953

Book review

W. G. Berl: **Physical Methods in Chemical Analysis,** Academic Press, Inc. 640 pages. Price $13.50, 1951.

As in Volume 1, each chapter in this book has been written by an expert in the field, and is concerned with a particular aspect of the use of physical methods in chemical analysis. The first chapter deals with polarography, and gives concise accounts of the theory, apparatus, and techniques used. Useful tables of depolarisation potentials are included, and over forty typical analyses are summarised. The chapter ends with a discussion of polarometric titrations. The basic features of polarography are adequately covered, and it is therefore unfortunate that only a few references to the available literature have been included for those who wish to follow the subject further. This is a general criticism of many chapters of the book. The next chapter covers the theory and technique of conductivity and conductometric titration. As a minor criticism one may note that the use of ion-exchange resins is not mentioned in the section on the preparation of conductivity water. The conductometric titration section includes phenols and alkaloids as well as inorganic acids and basis, and titrations which involve precipitations are also reviewed. Potentiometric analysis is discussed in an admirable manner in the following chapter, and adequate references to literature data and reference books are given.

An excellent account of electrography and electrospot testing includes a historical survey, full details, with good diagrams, of the equipment, materials, electrolytes, reagents, etc. used and a good review of uses in identification of pure metal surfaces, alloys, and anions. Special applications, such as the structure of steel and nonferrous metals, and a section on quantitative applications, complete this useful chapter. Adequate accounts of magnetic methods of analysis, and of the determination of the area of surfaces of solids, are followed by a chapter on surface tension measurements. This reviews competently the capillary rise, maximum bubble pressure, drop-weight and pendant drop, and ring methods of determination of surface tension, but would have been much improved by a detailed section on applications.

Vacuum techniques of analysis depend first on the production and measurement of low pressures, and a good, but perhaps over-long, account of this is given. The vacuum fusion method for the analysis of gaseous elements in metals, and the determination of carbon by low-pressure combustion are next considered in detail. The section on the micro-analysis of gases at low pressures covers only a small part of the field, however, although literature references are given to other work. A discussion of molecular distillation and a full collection of references completes this somewhat unbalanced chapter. A good account of analysis by thermal conductivity comes next, and is followed by a useful chapter on the measurement of radioactivity for tracer applications. This surveys, with the aid of excellent diagrams, the photographic and electric methods of detection, the principles of counting, and analytical procedures. An equally useful chapter is that on statistical analysis, with particular reference to spectrography and spectrographic analysis; numerical examples are given. The final chapters surveys briefly chromatographic analysis, and is useful as an introduction to the subject.

The book is well printed, is relatively free from major errors, and on the whole provides a valuable compendium of methods and techniques of physical methods of analysis which should be available in every library.

R. N. Haszeldine

CORRECTION

The condensation of vapour gas—vapour mixtures

The constants to use in the equation on page 137 of the June 1953 issue have been incorrectly evaluated. They should read :

for chloroform and air $K^1 = 6980$
for steam and air $K^1 = 9190$

This introduces an error in the application of the Colburn approximate design method to the author's results. The new constants result in the calculated areas being approximately 90 per cent greater than the experimental area for both systems instead of approximately 40 per cent as reported.

The conclusion that this method is conservative for the cases studied still applies.

R. C. Cairns

VOL. 2 1953

END